Cold Tongue and Warm Pool ENSO Events in CMIP5: Mean State and Future Projections

ANDRÉA S. TASCHETTO, ALEXANDER SEN GUPTA, NICOLAS C. JOURDAIN, AND AGUS SANTOSO

Climate Change Research Centre, and ARC Centre of Excellence for Climate System Science, University of New South Wales, Sydney, New South Wales, Australia

CAROLINE C. UMMENHOFER

Department of Physical Oceanography, Woods Hole Oceanographic Institution, Woods Hole, Massachusetts

MATTHEW H. ENGLAND

Climate Change Research Centre, and ARC Centre of Excellence for Climate System Science, University of New South Wales, Sydney, New South Wales, Australia

(Manuscript received 23 July 2013, in final form 12 November 2013)

ABSTRACT

The representation of the El Niño–Southern Oscillation (ENSO) under historical forcing and future projections is analyzed in 34 models from the Coupled Model Intercomparison Project phase 5 (CMIP5). Most models realistically simulate the observed intensity and location of maximum sea surface temperature (SST) anomalies during ENSO events. However, there exist systematic biases in the westward extent of ENSO-related SST anomalies, driven by unrealistic westward displacement and enhancement of the equatorial wind stress in the western Pacific. Almost all CMIP5 models capture the observed asymmetry in magnitude between the warm and cold events (i.e., El Niños are stronger than La Niñas) and between the two types of El Niños: that is, cold tongue (CT) El Niños are stronger than warm pool (WP) El Niños. However, most models fail to reproduce the asymmetry between the two types of La Niñas, with CT stronger than WP events, which is opposite to observations. Most models capture the observed peak in ENSO amplitude around December; however, the seasonal evolution of ENSO has a large range of behavior across the models. The CMIP5 models generally reproduce the duration of CT El Niños but have biases in the evolution of the other types of events. The evolution of WP El Niños suggests that the decay of this event occurs through heat content discharge in the models rather than the advection of SST via anomalous zonal currents, as seems to occur in observations. No consistent changes are seen across the models in the location and magnitude of maximum SST anomalies, frequency, or temporal evolution of these events in a warmer world.

1. Introduction

The environmental and societal impacts of the El Niño–Southern Oscillation (ENSO) set against a gradual warming of the background climate has prompted concerted efforts to improve our understanding of ENSO behavior. Our capacity to predict the onset and duration of ENSO events has benefitted from sustained observing systems (e.g., McPhaden et al. 1998) coupled with developments in ENSO theories (e.g., Jin 1997), as well as ongoing improvements of climate models such as those facilitated by the Climate Model Intercomparison Project (CMIP). In the present study, we assess the fidelity of climate models submitted to CMIP phase 5 (CMIP5) in simulating the interannual SST variability in the tropical Pacific that is largely associated with ENSO and examine how this variability is projected to change in the future.

Previous studies have shown that both atmospheric and oceanic signatures of ENSO events are asymmetric in intensity, frequency, duration, spatial distribution, and in their large-scale atmospheric responses. For

Corresponding author address: Andréa S. Taschetto, Climate Change Research Centre, and ARC Centre of Excellence for Climate System Science, University of New South Wales, Sydney NSW 2052, Australia.
E-mail: a.taschetto@unsw.edu.au

DOI: 10.1175/JCLI-D-13-00437.1

example, Hoerling et al. (1997) noted that the nonlinear response in Northern Hemisphere precipitation and atmospheric circulation to the warm and cold phases of the Southern Oscillation can be attributed to nonlinearities in deep convection to SST. Burgers and Stephenson (1999) reported a skewness in equatorial eastern Pacific SST anomalies that has shown to be related to the different air–sea feedback interactions during the warm and cold ENSO phases (Kang and Kug 2002; Frauen and Dommenget 2010). Other studies, on the other hand, attribute ENSO asymmetry to nonlinear oceanic processes (e.g., An and Jin 2004; Su et al. 2010). For instance, An and Jin attributed the warm–cold amplitude asymmetry to a strong nonlinear dynamic heating that enhances the warm events, as occurred in the 1982/83 and 1997/98 events, and weakens subsequent cold events.

The asymmetric characteristics of ENSO also manifest in the location of the associated maximum SST anomalies. Canonical El Niño events generally show largest SST anomalies in the eastern Niño-3 region. In contrast, La Niña anomalies tend to peak in the central Pacific, within the Niño-4 region (e.g., Schopf and Burgman 2006; Sun and Yu 2009). This spatial asymmetry may be partly related to the nonlinear wind stress response to SST anomalies associated with opposite phases of ENSO (e.g., Kang and Kug 2002; Frauen and Dommenget 2010; Dommenget et al. 2013).

The transition between ENSO phases occurs via a negative feedback involving ocean wave dynamics (e.g., Battisti and Hirst 1989; Suarez and Schopf 1988; Jin 1997). In a zonally integrated sense, the action of internal waves leads to a buildup of ocean heat content in the equatorial Pacific as El Niño develops and is subsequently drained off the equator, leading to a delayed negative feedback and phase reversal to La Niña conditions (Jin 1997). This so-called recharge–oscillator paradigm has been confirmed by observations (Meinen and McPhaden 2000) but can only explain the linear component of ENSO transitions (McGregor et al. 2013). In reality, the warm and cold event transition is not regular and ENSO events are also asymmetric in duration (e.g., Larkin and Harrison 2002; McPhaden and Zhang 2009; Okumura and Deser 2010; Ohba and Ueda 2009; Ohba et al. 2010; Okumura et al. 2011). Warm SST anomalies associated with strong El Niño events tend to decay relatively quickly after their peak in December and are followed by cold SST anomalies in the equatorial Pacific. On the other hand, strong La Niña events often persist through the following year.

In addition to the nonlinear duration between the Pacific warm and cold events, asymmetric behavior is also observed between strong and weak events of the same ENSO phase. Previous studies have identified inter–El Niño variations when the maximum SST anomalies concentrate in the central rather than the eastern Pacific. This central warming pattern appears as the second mode of tropical Pacific SST variability in an empirical orthogonal function (EOF) or rotated-EOF analysis (Lian and Chen 2012). Some studies have postulated that the first two modes of variability in tropical Pacific SST anomalies represent dynamically independent processes (e.g., Ashok et al. 2007). Others, however, argue that the central Pacific events can be considered as a nonlinear manifestation of the canonical ENSO (e.g., Trenberth and Smith 2009; Takahashi et al. 2011; Dommenget et al. 2013; Johnson 2013). Whether or not a separate mode to canonical ENSOs, these central Pacific events have drawn considerable attention as they have occurred more frequently in the past few decades (e.g., Ashok et al. 2007; Lee and McPhaden 2010; Na et al. 2011).

The mechanisms that give rise to enhanced central Pacific anomalies are still not fully understood. Ashok et al. (2007) proposed that the recent weakening of equatorial easterlies in the central Pacific and enhanced easterlies to the east have decreased the zonal SST gradient and flattened the thermocline, resulting in a climate state more favorable for the evolution of the central Pacific events. Choi et al. (2011, 2012) suggested that decadal changes in climate can play an important role in modulating the occurrence of El Niño with different warming signatures. It has been proposed that the asymmetries between the cold and warm phases of the Southern Oscillation may produce a nonzero residual effect on the time-mean state of the tropical Pacific that in turn modulates ENSO amplitudes (Yeh and Kirtman 2004; Rodgers et al. 2004). Sun and Yu (2009) suggested that the spatial asymmetries between El Niño and La Niña lead to an ENSO cycle that shifts the tropical Pacific mean climate from a state favorable for strong ENSO activity to a state that sustains weak ENSO activity, a mechanism that has been reproduced by 3 of 19 CMIP3 models according to Yu and Kim (2011).

Different names have been ascribed to central Pacific ENSO events, despite referring to essentially the same SST structure. We adopt the ''cold tongue'' (CT) and ''warm pool'' (WP) terminologies to refer to ENSO events with maximum SST anomalies located in the eastern and central equatorial Pacific, respectively: CT El Niño, CT La Niña, WP El Niño, and WP La Niña. Regardless of whether the CT and WP events are independent modes of variability or a manifestation of ENSO nonlinearity, observations demonstrate that such spatial asymmetries are part of the interannual variability of the region and that distinct atmospheric

teleconnections and associated climate impacts arise when SST peaks in the central or eastern Pacific (e.g., Ashok et al. 2007; Weng et al. 2007; Taschetto and England 2009; Taschetto et al. 2009, 2010). As such, it is important that climate models simulate the characteristics of these different ENSO flavors.

Despite significant advances in climate models, simulating realistic ENSO characteristics is still a major challenge (Guilyardi et al. 2009b), largely associated with the difficulty in representing multiple competing feedback processes (e.g., Collins et al. 2010; Kim and Jin 2011; Bellenger et al. 2013). Leloup et al. (2008) assessed 23 CMIP3 models and concluded that the majority of the models are not able to simulate the location of maximum amplitude of warm and cold events; only half can properly simulate ENSO onset, and none can represent the correct termination phases of either El Niño or La Niña. Nevertheless, climate models have shown some improvements in simulating ENSO-related SST variability and trends since CMIP3 (e.g., Yu and Kim 2010; Kim and Yu 2012; Bellenger et al. 2013; Guilyardi et al. 2012; Yeh et al. 2012; Jourdain et al. 2013).

The relatively short observational record available to date means that understanding the dynamics behind WP ENSO events, which have become more frequent in recent decades, relies more on the use of climate models (e.g., Dewitte et al. 2012). Sparse observational records and the lack of a dynamical theory also imply uncertainty in determining whether the recent increase in the frequency of WP relative to CT El Niño can be attributed to greenhouse warming (Wittenberg 2009; McPhaden et al. 2011; Newman et al. 2011; Yeh et al. 2011; Kim et al. 2012). Assessing how well the CMIP models capture the observed temporal and spatial characteristics of ENSO may help to clarify the dynamics underlying the two types of ENSO as well as their future projections. Here we use a large pool of available CMIP5 models to provide a comprehensive assessment on their performance in representing the two types of ENSO regarding 1) their spatial characteristics; 2) their associated atmospheric, ocean surface, and subsurface properties; 3) their evolution and seasonality; and 4) their projections in a warmer climate scenario.

2. Models and methods

a. Observations and reanalysis data

The SST dataset used here is the Hadley Centre Sea Ice and Sea Surface Temperature dataset version 1 (HadISST1) (Rayner et al. 2003). Wind stress data are from the National Centers for Environmental Prediction–National Center for Atmospheric Research (NCEP–NCAR) reanalysis (Kalnay et al. 1996). In this study, we consider the period from December 1949 to November 2012 for the SST and wind stress fields.

Subsurface ocean temperature data is from the Simple Ocean Data Assimilation (SODA version 2.1.6) reanalysis (Carton and Giese 2008), covering the period from December 1958 to November 2008. The upper-ocean heat content accumulated in the top 300 m averaged between 3°S and 3°N is used as a proxy for the equatorial Pacific thermocline depth (Zebiak 1989).

b. CMIP5 models

We analyze outputs from 34 climate models taking part in CMIP5 that were used to inform the Intergovernmental Panel on Climate Change (IPCC) Fifth Assessment Report (AR5). A summary of the climate models is shown in Table 1.

We examine two scenarios in this study: 1) historical simulations, which are integrations from around 1850 to at least 2005 using realistic natural and anthropogenic forcings, and 2) representative concentration pathway 8.5 (RCP8.5) simulations, which are subject to increasing radiative forcing from the end of the historical simulation to 2100 when the radiative forcing reaches $\sim$8.5 W m^{-2}. The last 50 years of the twenty-first century are analyzed in the RCP8.5 simulations. A description of the CMIP5 experiment design can be found in Taylor et al. (2012).

c. Methodology

For all variables, anomalies are calculated by removing the long-term monthly climatology over the entire period analyzed here. Time series of observations and simulations are then linearly detrended. When required, 3-month averages are calculated for the examination of particular seasons: namely, December–February (DJF), March–May (MAM), June–August (JJA), and September–November (SON).

When a mean across all CMIP5 models is considered, the spatial fields are interpolated onto a common $1° \times 1°$ grid for comparison with observations. Ensemble members for individual models are averaged prior to computing multimodel mean.

Where necessary, the estimate of the confidence levels or spread across CMIP5 models is calculated via the standard deviation among the models. The estimate of significance levels is computed via null hypothesis using a Student's t test at the 0.05 significance level.

The selection of ENSO years is based on the DJF season, when observed events typically peak. Classifying ENSO events in models can be challenging, as models contain spatial SST biases. However, defining

TABLE 1. List of the CMIP5 models, with respective institutes, variables, and number of ensemble members used in this study.

Model acronym	Model	Institute, country	Variables				
			SST		Wind stress	Subsurface temperature	Thermocline
			HIST	RCP8.5			
ACCESS1.0	Australian Community Climate and Earth-System Simulator, version 1.0	Commonwealth Scientific and Industrial Research Organisation (CSIRO)–Bureau of Meteorology (BOM), Australia	1	1	1	1	1
ACCESS1.3	Australian Community Climate and Earth-System Simulator, version 1.3	BOM, Australia	1	1	1	1	1
BCC-CSM1.1	Beijing Climate Center, Climate System Model, version 1.1	Beijing Climate Center (BCC), Chinese Meteorological Administration (CMA), China	3	1	3		
CanESM2	Second Generation Canadian Earth System Model	Canadian Centre for Climate Modelling and Analysis (CCCma), Canada	5	5	3	1	1
CESM1 (CAM5)	Community Earth System Model, version 1 (Community Atmosphere Model, version 5)	National Science Foundation (NSF)–U.S. Department of Energy (DOE)–NCAR, United States	2	3			
CESM1 (FASTCHEM)	Community Earth System Model, version 1 (with FASTCHEM)	NSF–DOE–NCAR, United States	3				
CESM1 (WACCM)	Community Earth System Model, version 1 [with the Whole Atmosphere Community Climate Model (WACCM)]	NSF–DOE–NCAR, United States	1	1			
CCSM4	Community Climate System Model, version 4	NCAR, United States	4	1	1	1	1
CMCC-CM	Centro Euro-Mediterraneo per I Cambiamenti Climatici Climate Model	Centro Euro-Mediterraneo per I Cambiamenti Climatici (CMCC), Italy	1	1			
CNRM-CM5	Centre National de Recherches Météorologiques Coupled Global Climate Model, version 5	Centre National de Recherches Météorologiques (CNRM)–Centre Européen de Recherche et de Formation Avancée en Calcul Scientifique (CERFACS), France	10	5	9	9	9
CSIRO Mk3.6.0	Commonwealth Scientific and Industrial Research Organisation Mark, version 3.6.0	CSIRO–Queensland Climate Change Centre of Excellence (QCCCE), Australia	10	10	10	10	10
FGOALS-g2	Flexible Global Ocean–Atmosphere–Land System Model gridpoint, version 2	State Key Laboratory of Numerical Modeling for Atmospheric Sciences and Geophysical Fluid Dynamics (LASG)–Center for Earth System Science (CESS), China	2		2		
FGOALS-s2	Flexible Global Ocean–Atmosphere–Land System Model, second spectral version	LASG–Institute of Atmospheric Physics (IAP), China	2	2			
FIO-ESM	First Institute of Oceanography (FIO) Earth System Model (ESM)	FIO, State Oceanic Administration (SOA), China	3	3			
GFDL CM3	Geophysical Fluid Dynamics Laboratory Climate Model, version 3	National Oceanic and Atmospheric Administration (NOAA)/Geophysical Fluid Dynamics Laboratory (GFDL), United States	5	1		1	1
GFDL-ESM2G	Geophysical Fluid Dynamics Laboratory Earth System Model with Generalized Ocean Layer Dynamics (GOLD) component	NOAA/GFDL, United States	1	1		1	1

TABLE 1. (*Continued*)

Model acronym	Model	Institute, country	Variables				
			SST		Wind stress	Subsurface temperature	Thermocline
			HIST	RCP8.5			
GFDL-ESM2M	Geophysical Fluid Dynamics Laboratory Earth System Model with Modular Ocean Model 4 (MOM4) component	NOAA/GFDL, United States	1	1		1	1
GISS-E2-H	Goddard Institute for Space Studies Model E2, coupled with the Hybrid Coordinate Ocean Model (HYCOM)	National Aeronautics and Space Administration (NASA) Goddard Institute for Space Studies (GISS), United States	5		2	1	1
GISS-E2-R	Goddard Institute for Space Studies Model E2, coupled with the Russell ocean model	NASA GISS, United States	5		1		
HadCM3	Hadley Centre Coupled Model, version 3	Met Office (UKMO) Hadley Centre, United Kingdom	9		4	4	4
HadGEM2-AO	Hadley Centre Global Environment Model, version 2–Atmosphere and Ocean	National Institute of Meteorological Research (NIMR), Korea Meteorological Administration (KMA), South Korea	1	1			
HadGEM2-CC	Hadley Centre Global Environment Model, version 2–Carbon Cycle	UKMO Hadley Centre, United Kingdom	2	3	2	1	1
HadGEM2-ES	Hadley Centre Global Environment Model, version 2–Earth System	UKMO Hadley Centre, United Kingdom	2	4	2	1	1
INM-CM4.0	Institute of Numerical Mathematics Coupled Model, version 4.0	Institute of Numerical Mathematics (INM), Russia	1	1	1	1	1
IPSL-CM5A-LR	L'Institut Pierre-Simon Laplace Coupled Model, version 5A, coupled with Nucleus for European Modelling of the Ocean (NEMO), low resolution	L'Institut Pierre-Simon Laplace (IPSL), France	4	4	4	2	2
IPSL-CM5B-LR	L'Institut Pierre-Simon Laplace Coupled Model, version 5B, coupled with NEMO, low resolution	IPSL, France	1	1		1	1
IPSL-CM5A-MR	L'Institut Pierre-Simon Laplace Coupled Model, version 5A, coupled with NEMO, mid resolution	IPSL, France	1	1	1	1	1
MIROC5	Model for Interdisciplinary Research on Climate, version 5	Atmosphere and Ocean Research Institute (AORI)–National Institute for Environmental Studies (NIES)–Japan Agency for Marine-Earth Science and Technology (JAMSTEC), Japan	3	3	3	1	1
MIROC-ESM	Model for Interdisciplinary Research on Climate, Earth System Model	AORI–NIES–JAMSTEC, Japan	3		3	3	3
MPI-ESM-LR	Max Planck Institute Earth System Model, low resolution	Max Planck Institute for Meteorology (MPI-M), Germany	3	3		3	3
MPI-ESM-MR	Max Planck Institute Earth System Model, medium resolution	MPI-M, Germany	3	1		1	1
MRI-CGCM3	Meteorological Research Institute Coupled Atmosphere–Ocean General Circulation Model, version 3	Meteorological Research Institute (MRI), Japan	3	1	3	1	1

TABLE 1. (*Continued*)

Model acronym	Model	Institute, country	Variables				
			SST		Wind stress	Subsurface temperature	Thermocline
			HIST	RCP8.5			
NorESM1-M	Norwegian Earth System Model, version 1 (intermediate resolution)	Norwegian Climate Centre (NCC), Norway	3	1	3	1	1
NorESM1-ME	Norwegian Earth System Model, version 1 (intermediate resolution) with interactive carbon cycle	NCC, Norway	1	1			

model-specific ENSO classifications to take into account model biases introduces subjective decisions. In addition, allowing multiple ENSO classifications would make model–observation intercomparison more difficult. As such, we adopt one common classification based on the state of equatorial Pacific SST anomalies. Even for observations, there is still no single method to classify two types of the El Niño pattern (e.g., Ashok et al. 2007; Yeh et al. 2009).

Here we adopt the method of Ham and Kug (2012) to classify ENSO events. The normalized DJF-averaged Niño indices are used as follows: An event is considered a CT El Niño if the Niño-3 index is greater than one standard deviation and the averaged SST anomaly in the Niño-3 region has a larger magnitude than the Niño-4 SST anomaly. An event is classified as WP El Niño if the Niño-4 index is above one standard deviation and the magnitude of the SST anomaly in the Niño-4 region is larger than in Niño-3. The opposite is used for La Niña events. Table 2 summarizes the ENSO classification for the purpose of this paper and shows the years of different types of ENSO events from the observations. ENSO events are selected for individual members of each CMIP5 model when more than one ensemble simulation is available.

Our analysis simplifies ENSO spatial pattern into CT and WP categories. This does not imply that these different ENSO flavors are related to distinct dynamical modes or that ENSO patterns are strictly bimodal. This is just a convenient way to examine differences in simulated ENSO characteristics (compared to the observations) when the primary variability is shifted more to the east or west.

To provide quantitative measures of the spatial structure of different ENSO flavors, we calculate the magnitude and location of the maximum SST anomaly (SSTA) along the equator, as well as the westward extent of the warm or cold anomalies. A model is considered to overestimate or underestimate the magnitude of El Niño or La Niña events if $|\mathrm{SSTA}|^{\max}_{\mathrm{model}}$ exceeds ($|\mathrm{SSTA}|^{\max}_{\mathrm{observed}} + \sigma^{\mathrm{SSTA}}_{\mathrm{observed}}$), where $|\mathrm{SSTA}|^{\max}_{\mathrm{model}}$ and $|\mathrm{SSTA}|^{\max}_{\mathrm{observed}}$ are the maximum magnitude of the SST anomaly composites along the equator (meridionally averaged between 5°S and 5°N) for the models and observations, respectively, and $\sigma^{\mathrm{SSTA}}_{\mathrm{observed}}$ is the standard deviation of the maximum SST anomaly over all events included in the observational composite. Similarly, a model is considered to have a ''realistic'' representation of the ENSO position if the longitude of the maximum SST anomaly falls within one standard deviation of the mean longitude of the observed composite events. The metric for the westward extent of the SST anomalies is defined as the most westward longitude where SSTA drops to half of

TABLE 2. Summary of criteria employed for the ENSO classification for observations and CMIP5 models, using the standardized DJF Niño-3 and Niño-4 indices. Years refer to January–February. For further details see text.

Event	Criteria	Years selected in observations
Cold tongue El Niño	Niño-3 > 1.0 and Niño-3 > Niño-4	1966, 1973, 1983, 1987, 1992, and 1998
Warm pool El Niño	Niño-4 > 1.0 and Niño-4 > Niño-3	1958, 1969, 1988, 1995, 2003, and 2010
Cold tongue La Niña	Niño-3 < −1.0 and Niño-3 < Niño-4	1950 and 1985
Warm pool La Niña	Niño-4 < −1.0 and Niño-4 < Niño-3	1956, 1971, 1974, 1976, 1989, 1999, 2000, 2001, 2008, 2011, and 2012

its maximum value. Note that, although this metric can be subjective, it is not restrictive in the sense that it accounts for spatial biases in each model in terms of the magnitude of ENSO SST.

3. Results

a. Number of ENSO events

Figure 1 shows the number of events for each ENSO type based on the historical simulations for each model, the multimodel mean, and observations. To facilitate comparison between models and with observations, the number of events are shown per 100 years. For most of the models, the number of El Niño events is comparable to the observations. For instance, there is a median of 11 CT El Niño events $(100\,\mathrm{yr})^{-1}$ in historical simulations versus approximately 10 events $(100\,\mathrm{yr})^{-1}$ in observations. There are 10 WP El Niño $(100\,\mathrm{yr})^{-1}$ in both simulations and observations. The number of La Niña events is not as well captured as for El Niño: there are 12

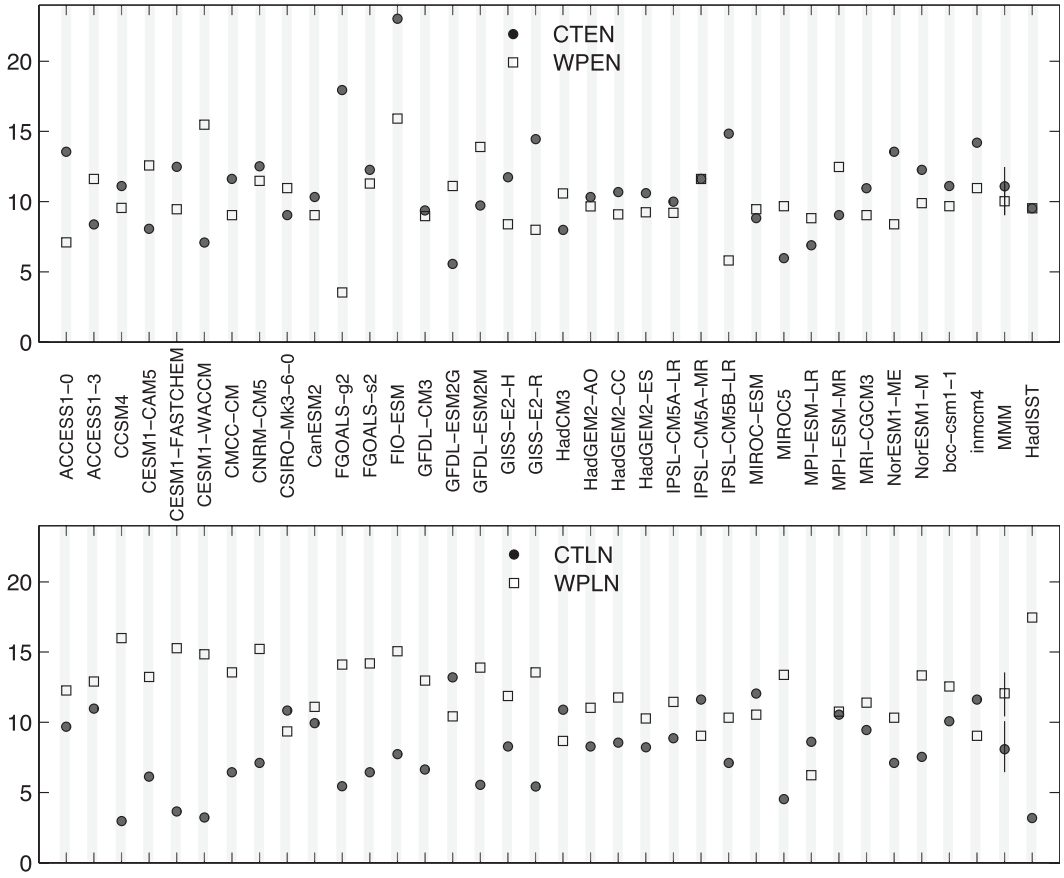

FIG. 1. Number of ENSO events $(100\,\mathrm{yr})^{-1}$ in the historical simulations for each model, multimodel mean, and observations. Number of events is averaged for models containing more than one member. (top) Warm events: CT El Niño (CTEN) represented by black circles and WP El Niño (WPEN) by white squares. (bottom) Cold events: CT La Niña (CTLN) represented as black circles and WP La Niña (WPLN) as white squares. Bars in the multimodel mean indicate the interquartile range.

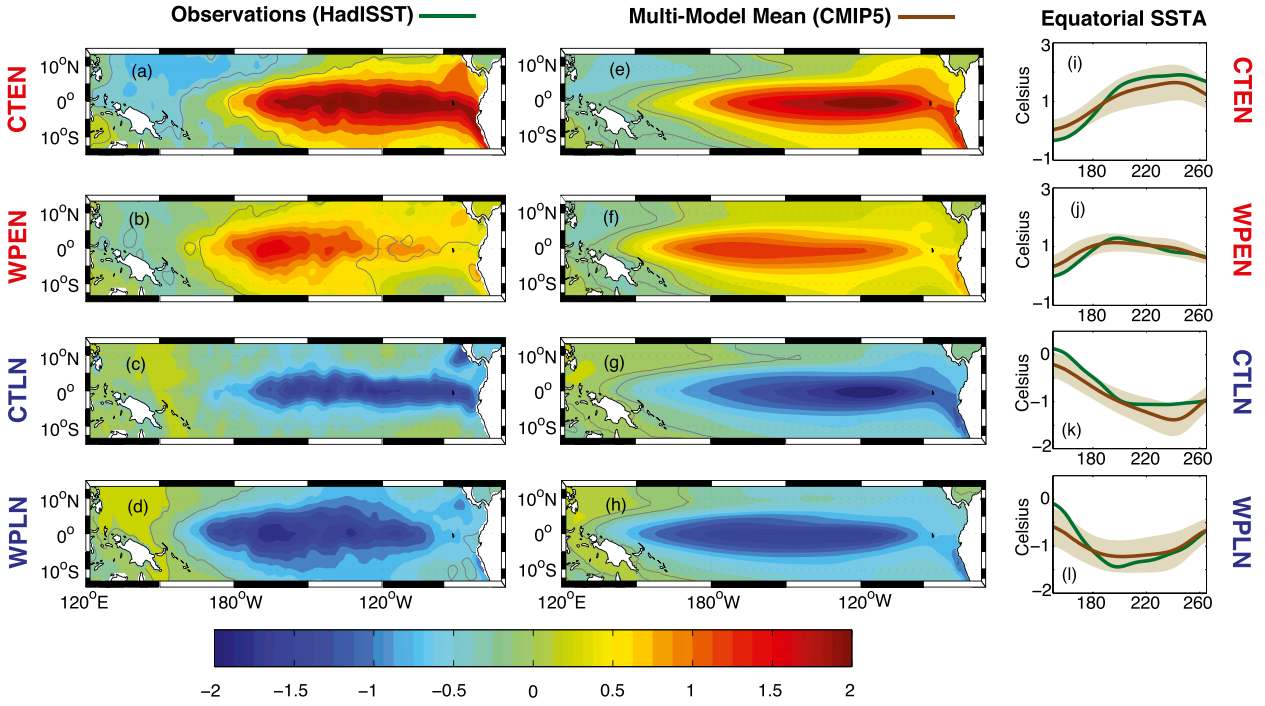

FIG. 2. Composite of SST anomalies (°C) during the December–February season for ENSO events. (left) Observations from HadISST based on the period December 1949–November 2012. (center) Multimodel mean based on 34 CMIP5 models. Areas within the thin gray line are statistically significant across the observed events and the composited events of CMIP5 models at the 0.05 significance level based on a Student's *t* test. (right) The December–February SST anomalies averaged over 5°S–5°N. The brown line represents the multimodel mean, while the green line represents observations. The light brown shading indicates the standard deviation of simulated composites, an estimate of the spread among CMIP5 models.

WP La Niña events $(100\,\mathrm{yr})^{-1}$ in simulations versus 17 events $(100\,\mathrm{yr})^{-1}$ in observations, and the median number of simulated CT La Niña events $(100\,\mathrm{yr})^{-1}$ is 8, while the observed number is only 3 events $(100\,\mathrm{yr})^{-1}$. Despite overestimating the number of CT La Niñas and underestimating the number of WP La Niñas, the observed asymmetry in the number of cold events is represented in most of the models, with more WP than CT La Niña events.

The number of observed ENSO events shown in Fig. 1 suggests that the separation of cold events into CT and WP La Niñas is more difficult than for warm events, agreeing with previous studies (e.g., Kug and Ham 2011). However, while there is a clear preference for WP to CT La Niña occurrence in observations, some CMIP5 models simulate similar numbers of the two types of cold events (e.g., CSIRO Mk3.6.0, CanESM2, HadCM3, the HadGEM2 models, the IPSL models, and MIROC-ESM). Only approximately one-third of the CMIP5 models simulate the observed preference for WP La Niña events: that is, CCSM4, the CESM models, CMCC-CM, CNRM-CM5, the FGOALS models, FIO-ESM, GFDL CM3, GFDL-ESM2M, GISS-E2-R, and MIROC5.

b. *Spatial pattern of ENSO*

The multimodel composite of simulated SST anomalies during austral summer (DJF) for both El Niño and La Niña events (Fig. 2, center) shows a number of features in common with the observations (Fig. 2, left). A quantification of the magnitude and location of the maximum SST anomaly as well as the westward extent of the ENSO pattern are presented in Fig. 3 for each model, the multimodel mean, and observations. The numbers of models that underestimate, overestimate, or "realistically" (see methods) represent the ENSO types are summarized in Table 3.

Most of the models simulate the magnitude of CT El Niño anomalies in the equatorial Pacific within the observational range. The magnitude of CT El Niño events is overestimated in only two models and underestimated in 11 models. This does not necessarily imply biases in the location or extension of SST anomalies during CT El Niño. In fact, the majority of the models (29 out of 34 models), regardless of the magnitude of maximum SST anomalies, simulate a realistic maximum SST anomaly position during CT El Niño events between 112° and

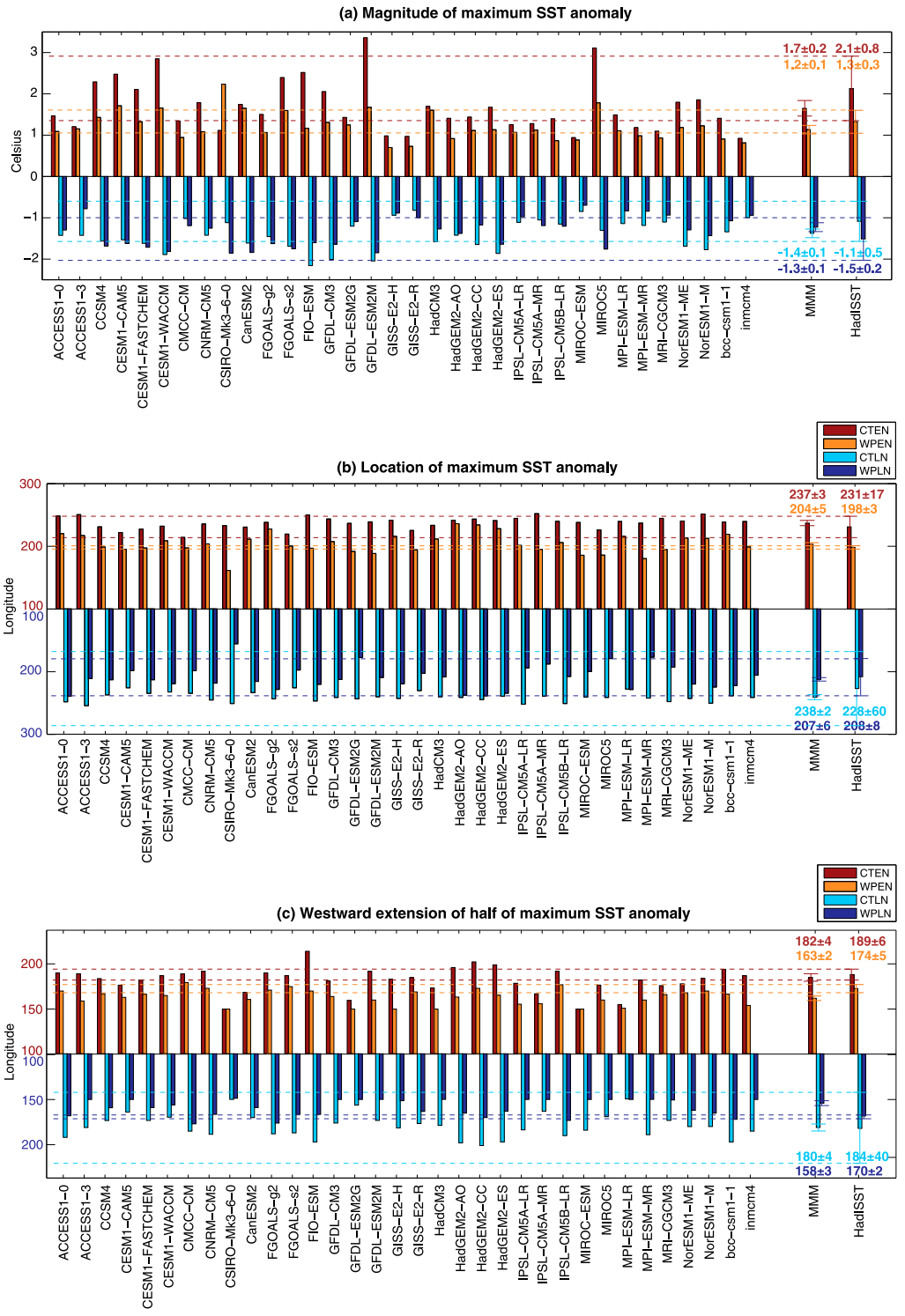

FIG. 3. (a) Magnitude and (b) location of the maximum SST anomaly for each ENSO type. (c) Westward extension of SST anomaly estimated as the location of half of the simulated maximum SST anomaly. Error bars (also represented as dashed lines) in HadISST show the 90% confidence interval for the mean of observed events. Error bars in the multimodel mean (MMM) represent the 90% confidence intervals for the mean of composited events across the CMIP5 models. The mean and associated error of each type of ENSO event are specified with the same color as in the legend for the MMM and observations. Models within the dashed lines are considered to have a realistic simulation of the metric.

TABLE 3. Number of models out of 34 that underestimate (↓), overestimate (↑), and reproduce "realistic" (′) types of ENSO. Largest numbers are in boldface. See methodology for explanation.

	CT El Niño			WP El Niño			CT La Niña			WP La Niña		
	↓	′	↑	↓	′	↑	↓	′	↑	↓	′	↑
Magnitude of max SST anomaly	11	**21**	2	10	**18**	6	0	**23**	11	8	**26**	0
Location of max SST anomaly	0	**29**	5	10	6	**18**	0	**34**	0	4	**30**	0
Extension of the western 0.5 times max magnitude	**16**	14	4	**24**	9	1	0	**34**	0	**28**	2	4

146°W (Table 3). However, the majority of the models have an extension bias with the warm pattern extending too far to the west. On the other hand, only four models reveal a CT El Niño pattern with an eastward bias: namely, FIO-ESM and the HadGEM2 models.

The bias in the westward extension and magnitude of SST anomalies is more severe for WP El Niño composites. In the observations the core of the warming is relatively narrow in the zonal direction (Fig. 2b), while the simulations reveal an elongated pattern with stronger anomalies (Fig. 2j). Only nine CMIP5 models can represent the relatively confined warming in the central Pacific (Figs. 2f,b, 3c) and only six of the models are able to simulate the maximum SST anomalies within the observed range (159°–165°W). Despite this, 18 out of 34 CMIP5 models simulate the magnitude of WP El Niño events within the observational range.

Despite biases in the magnitude and spatial extent of SST anomalies, all of the models (except CSIRO Mk3.6.0) reproduce the observed asymmetry between CT and WP warm events: they simulate relatively strong warm events in the east and relatively weak warm events in the west (Fig. 3a). The exception is the CSIRO Mk3.6.0 model that fails to capture the location and magnitude of maximum SST anomalies during WP El Niño events and simulates weaker SST conditions during CT instead of WP El Niño (i.e., the asymmetry is in the opposite sense to the observations).

While CMIP5 models simulate the observed asymmetry in magnitude between the two types of warm

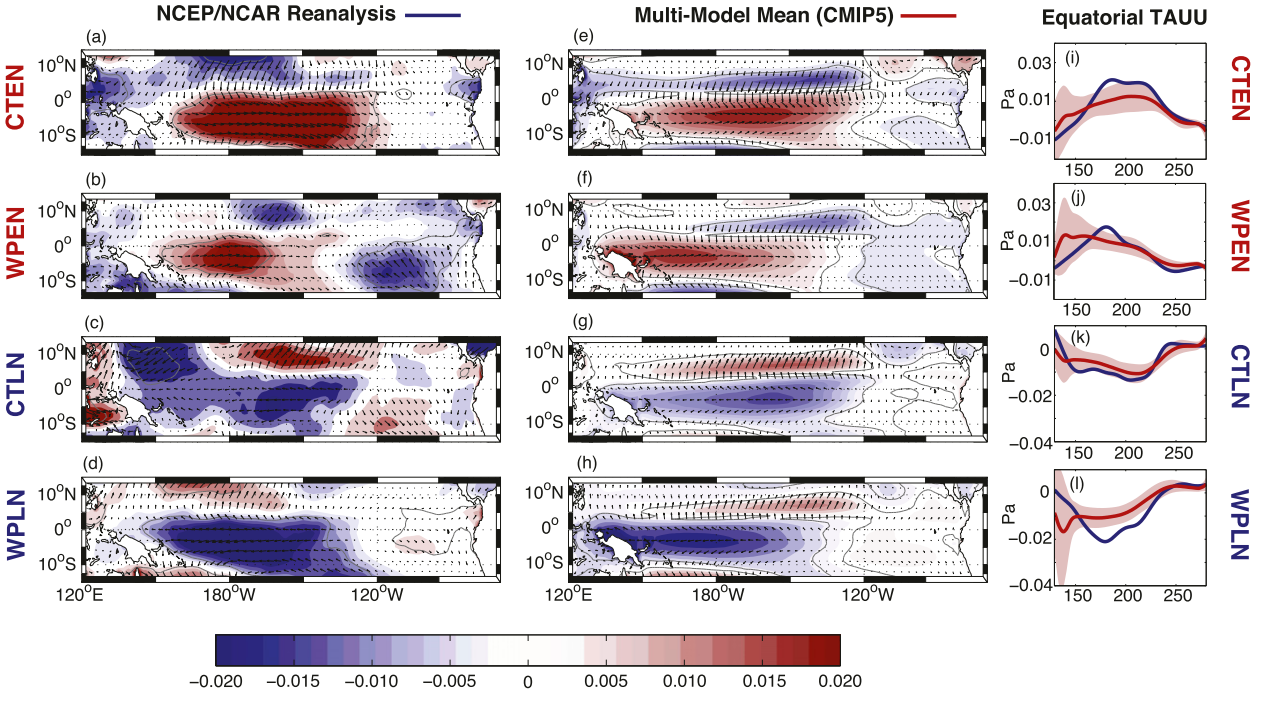

FIG. 4. Composite of wind stress anomalies (zonal component shaded) during the December–February season for ENSO events. Maximum vector length is 0.08 Pa. (left) NCEP–NCAR reanalysis. (center) Multimodel mean based on 20 CMIP5 models. Areas within the thin gray line are statistically significant across the observed events and the composited events of CMIP5 models at the 0.05 significance level based on a Student's *t* test. (right) The December–February zonal wind stress anomalies averaged over 3°S–3°N. The red (blue) line represents the multimodel mean (reanalysis). A 15° window running mean was applied to the curves. The light red shade indicates the standard deviation of simulated composites, an estimate of the spread among CMIP5 models.

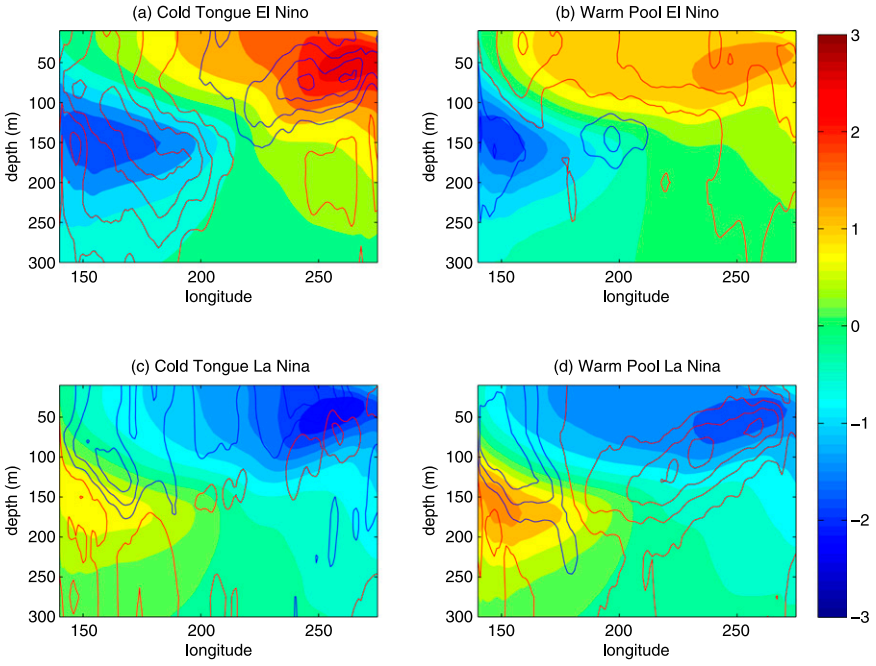

FIG. 5. Multimodel-mean ocean temperature anomalies (°C, shaded) averaged across 3°S–3°N along the Pacific during the December–February season for ENSO events: (a) cold tongue El Niño, (b) warm pool El Niño, (c) cold tongue La Niña, and (d) warm pool La Niña. The difference between the multimodel mean and observations are contoured in 0.3°C intervals. Red (blue) contours are positive (negative) differences. The multimodel mean is based on 23 CMIP5 models.

events, this is not the case for the cold events. In contrast to the observations, 22 out of 34 models simulate stronger CT events than WP La Niña (Figs. 2g,h, 3a). Nevertheless, the majority of the models (23 out of 34) are able to simulate CT La Niñas with a similar magnitude as in the observations (Fig. 2k). In addition, the location and westward extension of CT La Niña events are within the observational range for most CMIP5 models. It is important to note that, due to the small sample of observed CT La Niña events, the comparison with observations is limited.

There is a systematic bias in the extension of WP La Niña events, with 28 out of 34 models having cold anomalies that extend farther west than in the observations. The bias in intensity and spatial structure of cold events is reflected in the multimodel mean with minimum SST anomaly of −1.4°C at 122°W for CT La Niña (Figs. 2g,k) and −1.3°C at 153°W for WP La Niña (Figs. 2h,l) compared with −1.1°C at 132°W (Figs. 2c,k) and −1.5°C at 152°W (Figs. 2d,l) for observed CT La Niña and WP La Niña, respectively.

The pattern of SST changes during ENSO events is intimately tied to the changes in surface wind stress. As a result we examine the composite DJF wind stress anomalies for the different categories of ENSO (Fig. 4). The maximum westerly (easterly) wind stress anomalies in the central South Pacific during CT El Niño (La Niña) events are reproduced in the multimodel mean (Figs. 4a,e,i and 4c,g,k, respectively). Notable biases are, however, apparent. For instance, the CT ENSO in the models is associated with overall weaker than observed zonal wind stress anomalies (Figs. 4a,e,i and 4c,g,k), consistent with the weaker subsurface temperature and heat content anomalies in Figs. 5a,c and 6a,c. Large biases are found during WP ENSO, where zonal wind stress anomalies extend and peak in the far western Pacific just to the east of Papua New Guinea with a larger magnitude compared to reanalysis (Figs. 4b,f and 4d,h). The maximum wind stress anomalies are located around 145°E (multimodel mean) in the WP ENSO compared to 180° in the reanalysis (Figs. 4j and 4l).

The overestimated zonal wind stress anomalies over the western Pacific would generate excessive upwelling (downwelling) during WP El Niño (WP La Niña). This is consistent with the composites of subsurface temperature anomalies along the equator shown in Fig. 5b (Fig. 5d), which indicate colder (warmer) subsurface temperature in the western Pacific at the depth of the thermocline compared to reanalysis. Concurrently, the overly strong westerly (easterly) wind anomalies tend to excessively suppress (enhance) the climatological equatorial upwelling during WP El Niño (WP La Niña),

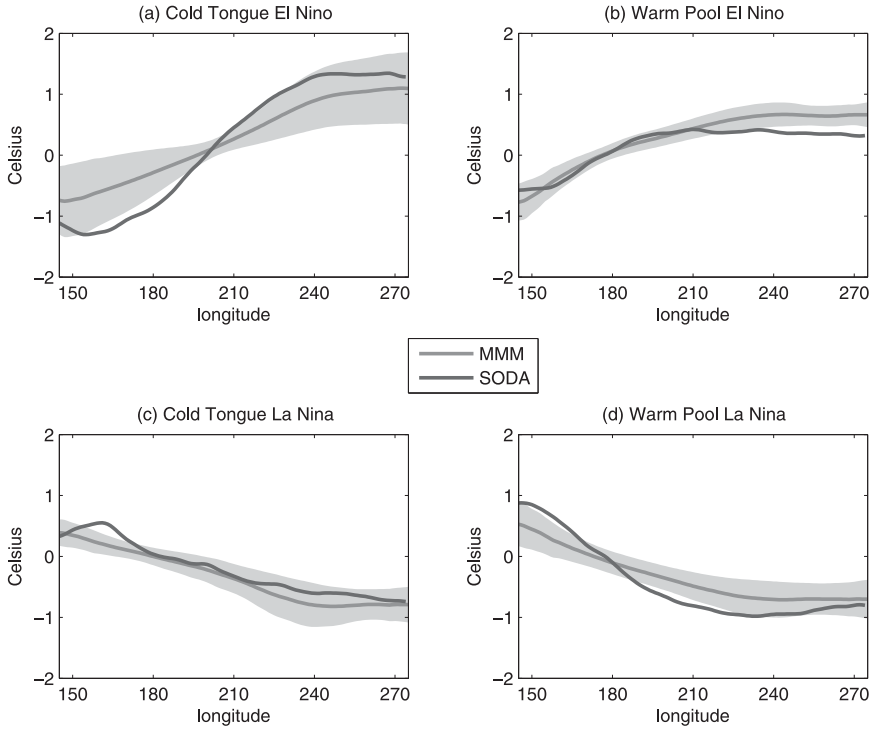

FIG. 6. Composite of ocean heat content anomalies averaged across 3°S–3°N along the Pacific and accumulated in the top 300 m during the December–February season for ENSO events: (a) cold tongue El Niño, (b) warm pool El Niño, (c) cold tongue La Niña, and (d) warm pool La Niña. The light gray curve is the multimodel mean heat content and the dark gray curve represents the SODA reanalysis. Light gray shade indicates the standard deviation of simulated composites, an estimate of the spread among CMIP5 models. The curves were smoothed with an 11° longitude point running mean. The multimodel mean is based on 23 CMIP5 models.

resulting in stronger warming (cooling) of the mixed layer over the west-central Pacific (Figs. 5b,d). The dynamical effect of the winds associated with WP El Niño is to shoal the thermocline, which in turn enhances stratification over the central Pacific, leading to cold subsurface and warm mixed layer biases (Fig. 6b). The reverse holds for WP La Niña (Fig. 6d). The overestimated wind stress in the western Pacific can also lead to a strengthened zonal current during WP events. Although the thermocline in the western Pacific is relatively deep, the zonal temperature gradients are generally strong, which could generate an efficient zonal advective feedback to produce excessive warming (or cooling) in that region during WP El Niños (La Niñas).

These wind stress biases allow the warm water to spread from the far west to the eastern equatorial Pacific during WP El Niño, as shown in the composite of subsurface temperature in Fig. 5b. In addition, the opposite pattern is seen for WP La Niña events (Fig. 5d) when biases in zonal wind stress anomalies intensify the easterlies too far west in the equatorial Pacific, allowing an unrealistic extension of cold waters in the equatorial Pacific. The response in the ocean surface is such that the associated SST anomaly is too intense in the western Pacific during WP La Niña events (Fig. 2l).

c. *Temporal evolution of ENSO*

The temporal evolution of SST, wind stress, and heat content anomalies associated with the four categories of ENSO are shown in Figs. 7–9 for the observations, reanalysis, and CMIP5 multimodel mean. The evolution of SST anomalies during ENSO events for individual models is presented in Fig. 10, where SST anomalies are averaged across the equatorial Pacific from 5°S to 5°N and from 150°E to 80°W. In Fig. 10, the evolution patterns are ordered according to the models that exhibit the highest to lowest correlations with the observed SST evolution.

In general the CMIP5 models correctly reproduce the timing of seasonal peaks in SST anomalies for all ENSO types (Figs. 9 and 10). However, there is a range of behavior in terms of duration of ENSO events and transition from warm to cold or neutral SST conditions (and vice versa). Here we describe the features associated with ENSO evolution separately for each type of event.

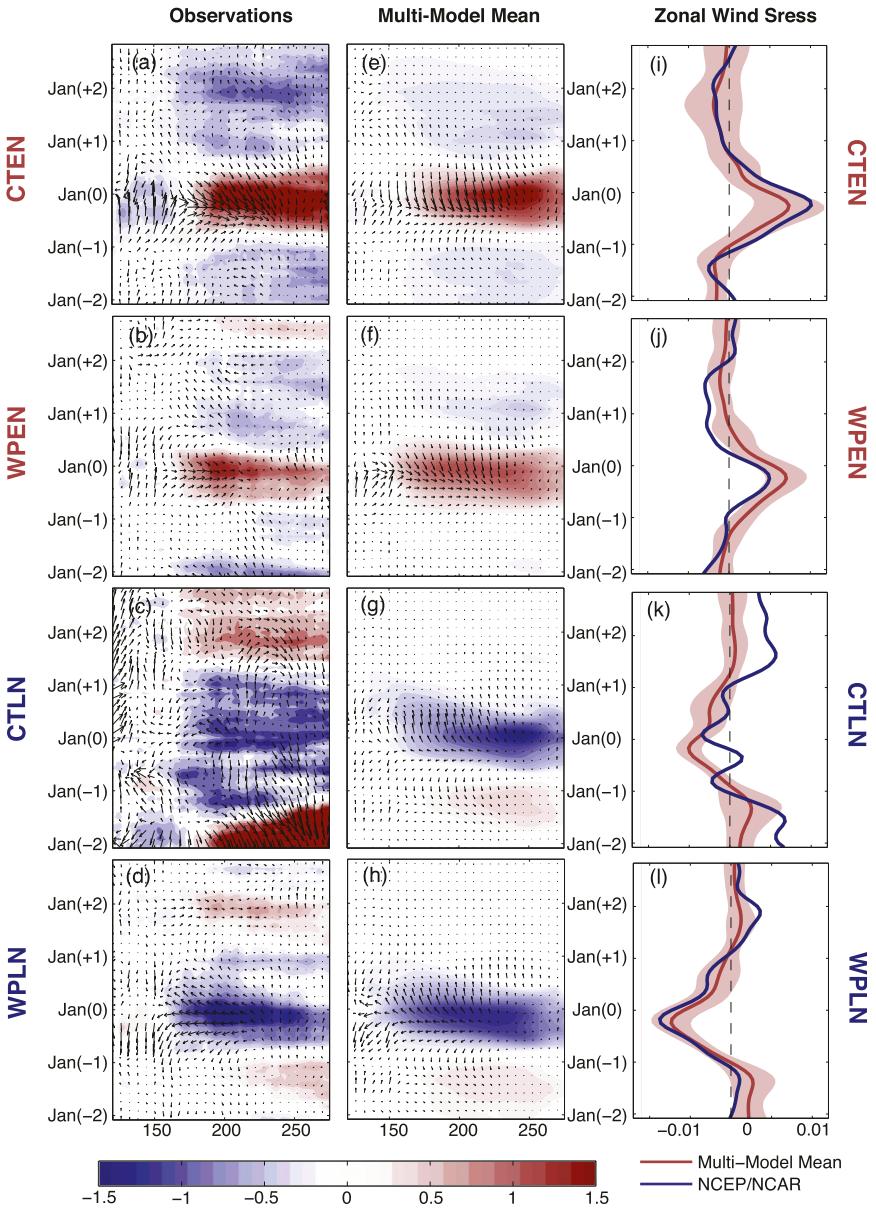

FIG. 7. Hovmoeller diagram of the SST (°C, shaded) and wind stress (Pa, vectors) anomalies averaged between 5°S and 5°N across the Pacific Ocean during ENSO events. Maximum vector length is 0.05 Pa. (left) Observations from HadISST dataset and reanalysis from NCEP–NCAR. (center) Multimodel mean of 20 CMIP5 models. (right) Evolution of zonal wind stress anomalies (Pa) averaged between 5°S and 5°N, 120°E and 110°W. The red (blue) line is the multimodel mean (NCEP–NCAR reanalysis), lines smoothed with an 11-month running mean. The light red area represents the standard deviation of the multimodel mean as an estimate of the spread across the models. (a),(e),(i) Cold tongue El Niño; (b),(f),(j) warm pool El Niño; (c),(g),(k) cold tongue La Niña; and (d),(h),(l) warm pool La Niña.

1) COLD TONGUE EL NIÑO

Overall, the multimodel mean evolution of CT El Niño events is well represented compared to observations. The SST anomalies in the equatorial Pacific become positive in February–March, peak in December, and vanish in October of the following year (Fig. 9a). As previously documented in the literature (e.g., Okumura and Deser 2010), CT El Niño events are generally followed by a La Niña event that starts in the following

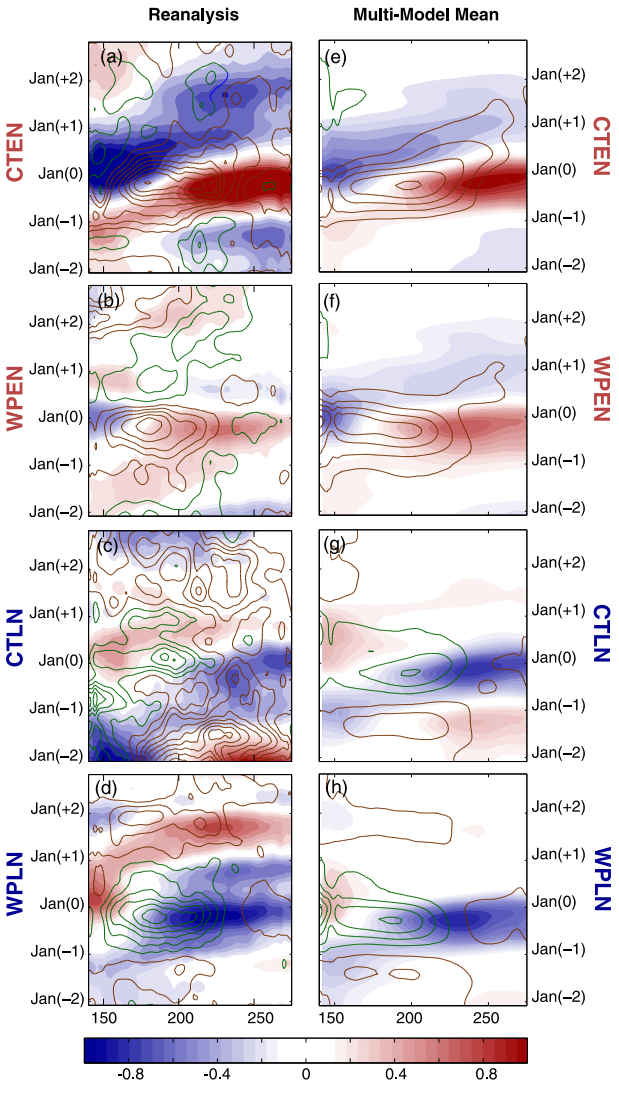

FIG. 8. Hovmoeller diagram of the ocean heat content (°C, shaded) and zonal wind stress (Pa, contours) anomalies averaged between 3°S and 3°N across the equatorial Pacific Ocean during ENSO events: (a),(e) cold tongue El Niño; (b),(f) warm pool El Niño; (c),(g) cold tongue La Niña; and (d),(h) warm pool La Niña. Brown (green) contours are westerly (easterly) anomalies, plotted at 0.003-Pa intervals. Multimodel mean of 16 CMIP5 models. An 11-month window running mean was applied to the data.

year but peaks in December, 2 yr after the maximum warming (Figs. 7a, 9a). CT El Niños are also generally preceded by cold anomalies 1 yr earlier. The evolution of observed CT El Niño events shown here is consistent with previous results based on the extended reconstructed SST, version 3 (ERSST.v3) data (Hu et al. 2012, their Fig. 3). The models exhibit this observed evolution with a wide range of fidelity. While some of the models tend to simulate CT El Niño events that are too long (lasting longer than 2 yr; e.g., GFDL-ESM2M, MIROC5, and MPI-ESM-LR), some exhibit a rapid transition to a strong La Niña with a seasonal cycle that is more extreme than in the observations [CCSM4, CESM1 (CAM5), CESM1 (FASTCHEM), CESM1 (WACCM), FIO-ESM, GFDL CM3, GFDL-ESM2M, and MIROC5; Fig. 10a]. Conversely, some models fail to simulate the transition from warm to cold events altogether (ACCESS1.0, IPSL-CM5A-LR, MIROC-ESM, MPI-ESM-MR, HadGEM2-AO, and INM-CM4.0).

The simulated CT El Niños are preceded and followed by much weaker than observed La Niñas (Figs. 7e and 7a). That the weak La Niña following a CT El Niño occurs 1 yr earlier than observed is apparently associated with the more rapid thermocline adjustment in the CMIP5 models (Figs. 8a,e), as indicated by the more rapid transition of the basinwide wind anomalies from westerly to easterly at the peak of El Niño (Fig. 7i), as well as the narrower meridional extent of the zonal winds compared to NCEP reanalysis (Figs. 4a,e). A narrower meridional extent of ENSO-related zonal wind anomalies would tend to generate faster off-equatorial Rossby waves, thus a more rapid phase transition (Kirtman 1997), which is a bias also seen in CMIP3 models (Capotondi et al. 2006).

2) WARM POOL EL NIÑO

The multimodel mean for the WP El Niño evolution captures the correct initiation and peak of SST anomalies in the central–western equatorial Pacific (Fig. 7f), with SST anomalies becoming positive around October and peaking in December of the following year (Fig. 9b). However, in most of the models, the SST anomalies associated with the simulated WP El Niño last longer (4 months longer in the multimodel mean, Fig. 9b) than observed events (Figs. 7b,f,j). For example, CanESM2 and HadCM3 simulate overly strong and prolonged WP El Niño events, followed by slightly cold anomalies in the following year (Fig. 10b). CCSM4, CESM1 (CAM5), CESM1 (FASTCHEM), GFDL-ESM2M, IPSL-CM5B-LR, and MIROC5 simulate prolonged warm SST anomalies in the Pacific, followed by strong cold anomalies 2 yr after the peak of WP El Niño events (Fig. 10b). A few models (MIROC-ESM and MPI-ESM-LR) represent WP El Niño with a much longer duration compared to observations and do not show a transition to SST anomalies of opposite sign either before or after the peak of the event (Fig. 10b).

Overall, the CMIP5 models simulate similar durations for WP and CT El Niño events. In observations, however, CT El Niños tend to last longer than WP El Niños (Figs. 7a,b) (Hu et al. 2012). This failure can be related to biases in the wind stress anomaly field in the western Pacific. Stronger than observed anomalous zonal wind

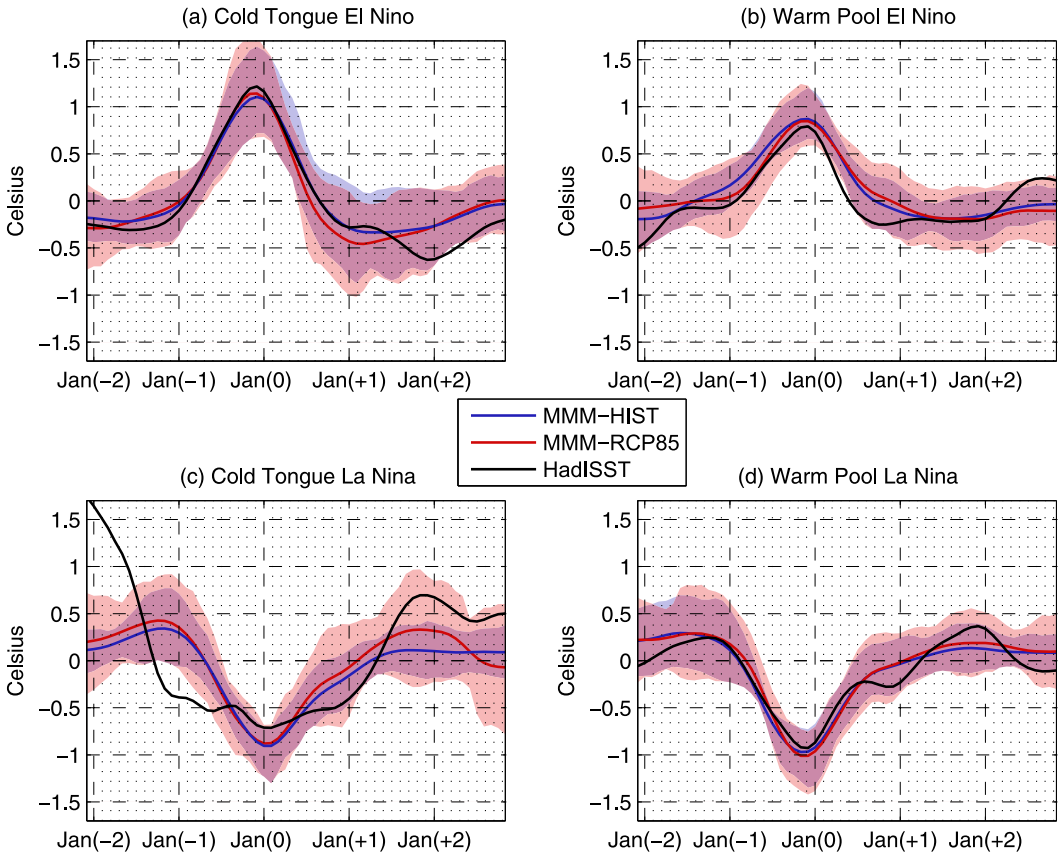

FIG. 9. Evolution of averaged SST anomalies averaged across the equatorial Pacific (5°S–5°N, 150°E–80°W): observations (black curve); multimodel mean of historical simulations (blue curve); and the multimodel mean of RCP8.5 scenario (red curve). Shading indicates the standard deviation of the multimodel mean for the historical (blue) and RCP8.5 (red) simulations. Composite for (a) cold tongue El Niño, (b) warm pool El Niño, (c) cold tongue La Niña, and (d) warm pool La Niña events.

stress is seen in the western Pacific approximately two seasons before the peak of the WP El Niño and lasts a couple of months after its mature phase (Figs. 7b,f). This results in a shallower than observed thermocline in the west during the austral summer season (Fig. 8b). It is currently thought that the spatial structure of WP El Niño does not favor a discharge process of the equatorial heat content that is efficient enough to trigger a cold event (Kug et al. 2009), which contrasts with CT El Niño events. Instead, the decay of WP El Niño is thought to be driven by zonal advection of mean SST gradients by anomalous zonal currents. However, the cold condition following the warm events and the eastward propagating negative thermocline anomalies in the multimodel mean (Fig. 8f) suggest that thermocline-related processes influence the evolution of WP El Niño in CMIP5 models to some degree. This is further supported by the southward shift of westerly anomalies at the peak of the simulated WP El Niños (marked by northerly anomalies across the equator in Fig. 4f). This feature, which is clear in CT but not WP El Niños in observations (Figs. 4a,b), is associated with heat content discharge (McGregor et al. 2012).

3) La Niña

The temporal evolution of La Niña events simulated by CMIP5 is remarkably similar between CT and WP events (Figs. 9c,d, 10c,d). Overall, the CMIP5 models simulate the peak of La Niña events at the correct season; however, the timing of the start of CT events is biased compared to observations (Figs. 9c, 10c). The multimodel mean evolution of CT La Niña shows a negative equatorial Pacific SST anomaly starting in April, that is, 7 months later than the observations (Figs. 7g,c, 9c), peaking correctly around January, and reaching neutral conditions in April of the following year (Fig. 9c).

In observations, CT La Niña events are preceded by warm SST conditions in the equatorial Pacific 2 yr before their peak (Figs. 7c, 9c, and 10c). CESM1 (CAM5) is the only model that correctly simulates the timing and magnitude of this warm event prior to CT La Niña

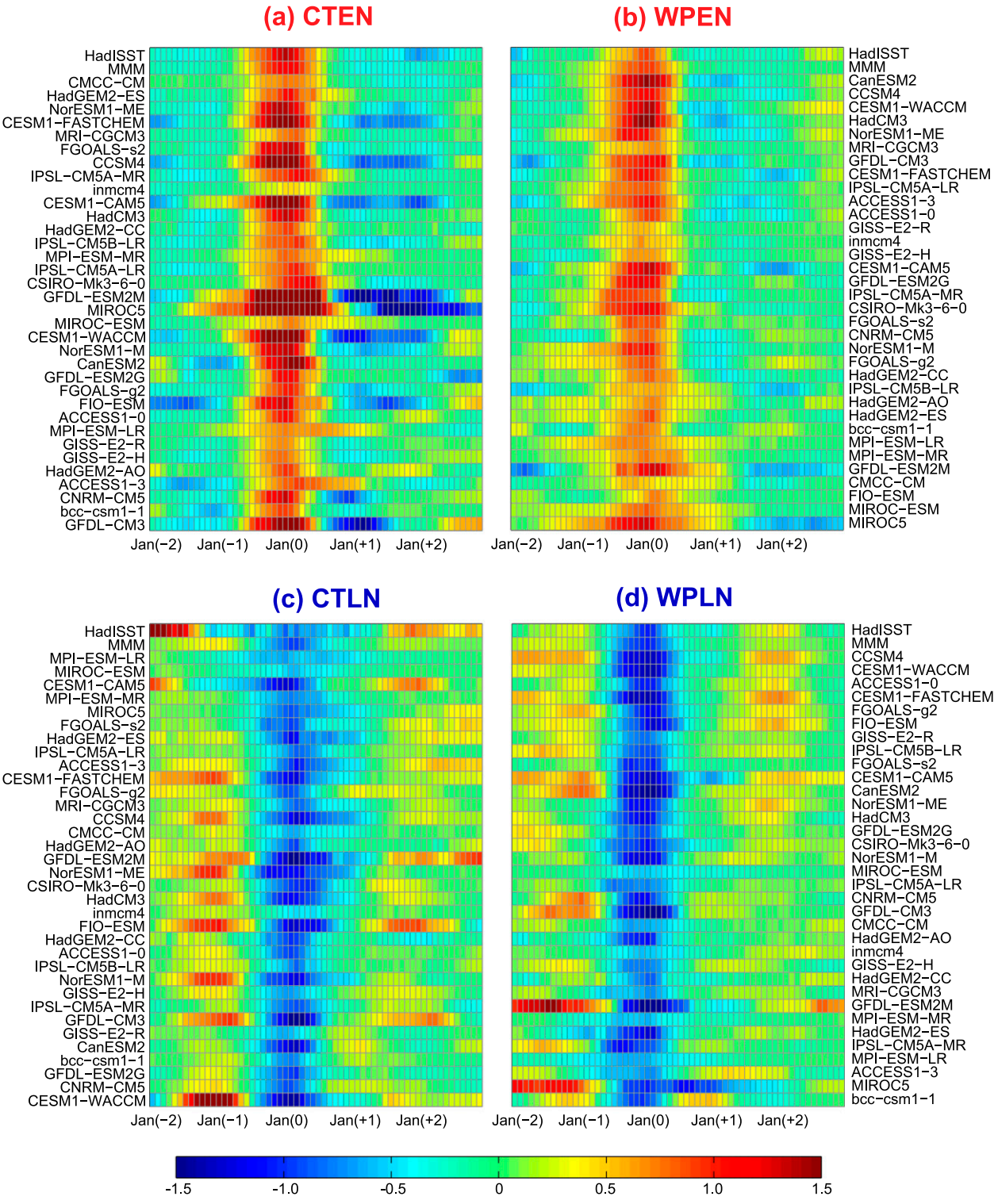

FIG. 10. Evolution of SST anomalies (°C) averaged across the equatorial Pacific (5°S–5°N, 150°E–80°W) for individual models: composite for (a) cold tongue El Niño, (b) warm pool El Niño, (c) cold tongue La Niña, and (d) warm pool La Niña events. Models are ordered according to correlations with observations.

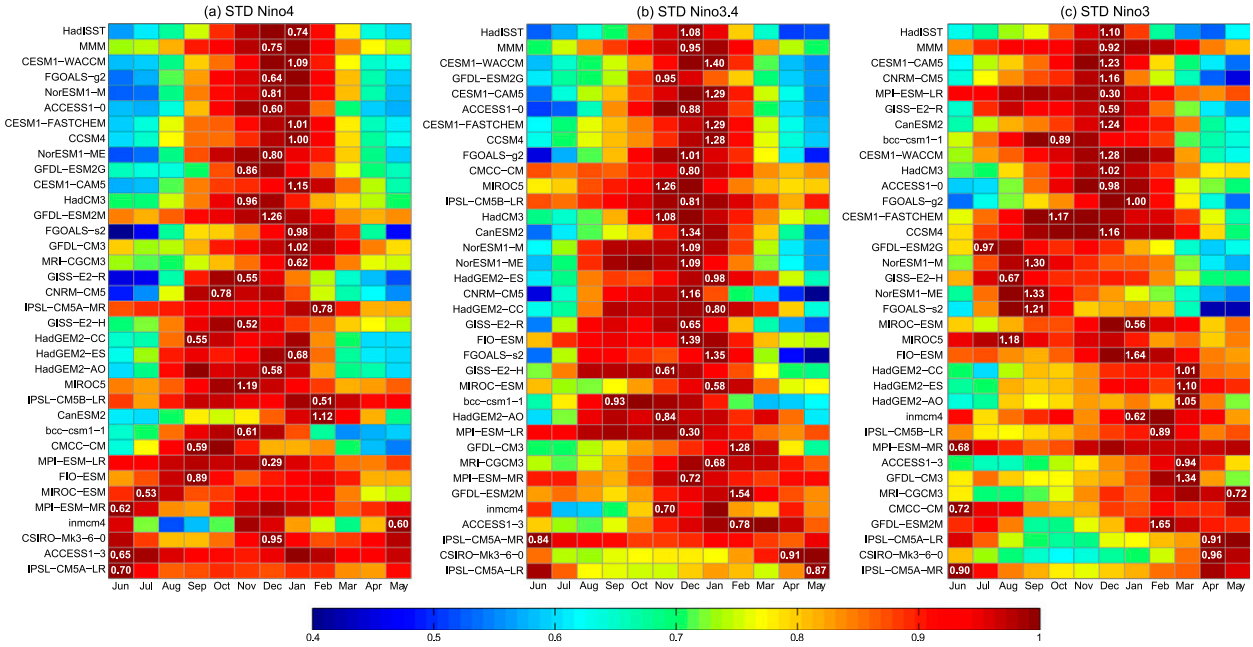

FIG. 11. Monthly standard deviation of (a) Niño-4, (b) Niño-3.4, and (c) Niño-3 indices for CMIP5 models. For comparison purposes, the monthly standard deviation is divided by the maximum value: this number is indicated in white in the month when it peaks. Models are ordered according to correlations with observations.

(Fig. 10c). In contrast, the CT La Niña events simulated by most of the CMIP5 models are preceded by a warming in the previous year (Figs. 7g, 8g, and 9c), particularly in CCSM4, CESM1 (FASTCHEM), CESM1 (WACCM), FIO-ESM, GFDL CM3, GFDL-ESM2M, HadCM3, NorESM1-M, and NorESM1-ME (Fig. 10c). It is important to note that a comparison of CT La Niñas between CMIP5 models and observations should be treated with caution given the small sample of observed events in the past 50 years.

Most of the models realistically simulate the timing of the initiation of WP La Niña events, with negative SST anomalies in the equatorial Pacific starting around March (Fig. 9d). However, most of the CMIP5 models do not reproduce the cold SST anomalies that last throughout the following year as in the observations (Figs. 7d,h, 8d,h), except CESM-CAM5 (Fig. 10d). Instead, the simulated multimodel mean WP La Niña events terminate 6 months earlier (Figs. 7h, 8h). The peak of observed and simulated WP La Niña events occurs in December and is preceded only by weak warm anomalies (Figs. 7d,h). Exceptions are GFDL-ESM2M and MIROC5 that simulate overly strong positive SST anomalies 2 yr before the peak of the WP cold event in the central Pacific (Fig. 10d).

The initiation timing of the zonal wind stress anomaly in the central equatorial Pacific is well captured in the multimodel mean (Fig. 7l). Unrealistically strong wind stress anomalies appear in the western Pacific (Fig. 7h), favoring a SST pattern that extends westward along the equator, as previously discussed. Additionally, the simulated wind stress anomaly persists throughout the year, resulting in a rapid thermocline adjustment (Fig. 8h) and an early termination of WP La Niña events in the CMIP5 models.

d. Seasonality of ENSO

Some of the biases seen in the evolution of warm and cold events may be related to an incorrect simulation of the seasonality of ENSO. Figure 11 displays the standard deviation of Niño indices for each model and observations. In general, most of the models show good fidelity in the timing and amplitude of SST variability in the central equatorial Pacific. Twenty-seven out of 34 CMIP5 models realistically represent the maximum amplitude of ENSO during November–January in the Niño-3.4 region (Fig. 11b). Greater disagreement is evident in the seasonality of ENSO in the eastern and western part of the tropical Pacific Ocean. For instance, only 13 out of 34 models capture the correct timing of maximum variability in the Niño-3 region. The discrepancies in the timing of the events among the models are reflected in the notably weaker multimodel mean ENSO seasonality compared to observations.

GFDL-ESM2M, GFDL CM3, and ACCESS1.3 exhibit maximum variability that is 2 months late for the Niño-3.4 region compared to observations, and the

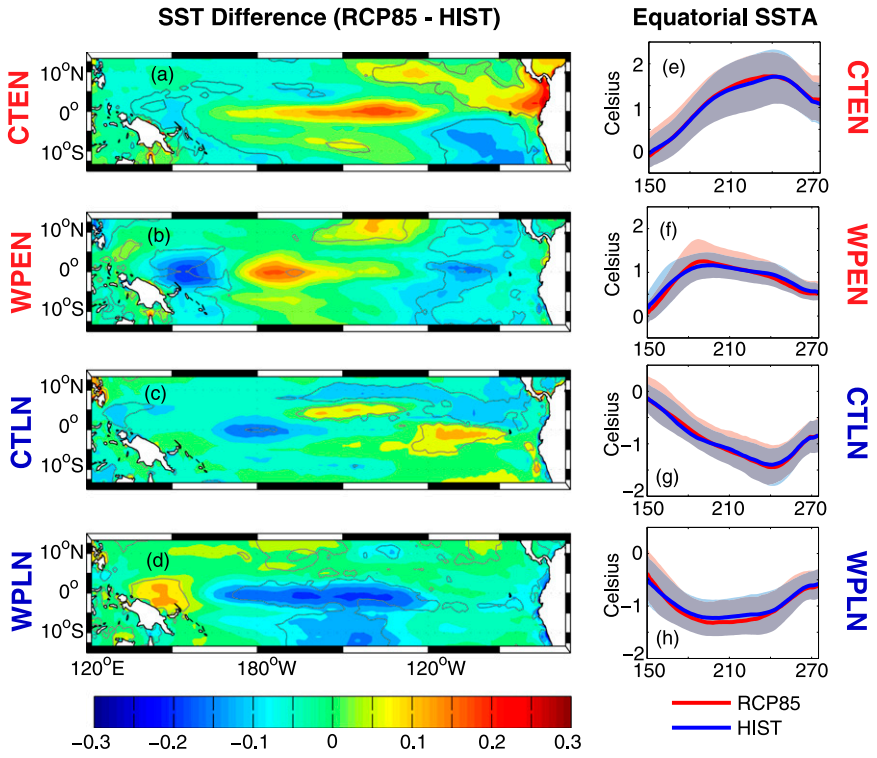

FIG. 12. (a)–(d) Difference in the simulated ENSO SST anomaly (°C) composites during the December–February season between the RCP8.5 and historical scenarios. Areas within the thin gray line are statistically significant at the 0.05 significance level based on a Student's *t* test. (e)–(h) SST anomaly averaged over the equatorial Pacific (5°S–5°N). The red (blue) line represents the multimodel mean for RCP8.5 (historical simulation). Light red (blue) shade indicates the standard deviation of simulated composites for the RCP8.5 (historical), an estimate of the spread among CMIP5 models of each scenario. Based on 27 CMIP5 models.

BCC-CSM1.1 is 3 months too early. This phase bias is even more extreme in some models, in particular IPSL-CM5A-MR, IPSL-CM5A-LR, and CSIRO Mk3.6.0, where the maximum variability occurs approximately 6 months after the observed peak of ENSO. In addition to representing ENSO events in the wrong season, the IPSL-CM5A-MR model has very weak seasonality, which is also true for FIO-ESM, MPI-ESM-LR, MPI-ESM-MR, IPSL-CM5B-LR, and CMCC-CM, although the ENSO indices in these models tend to peak in the correct season. These results are consistent with Bellenger et al. (2013).

As shown in this analysis, the substantial spread in the seasonal peak of warm and cold events compared to observations suggests that ENSO timing is one of the aspects requiring improvement in future CMIP simulations.

4. Future projections

Here we analyze how the different types of ENSO events may change in the future as projected by 27 CMIP5 models that had archived RCP8.5 simulations at the time of writing. Figure 12 shows the multimodel mean difference in equatorial Pacific SST anomalies between the RCP8.5 and historical simulations for each type of event. For the CT El Niños, the multimodel mean shows significant cooling in the eastern South Pacific and western Pacific but a warming in the eastern North Pacific (Fig. 12a). The WP El Niños reveal a slight warming in the central–west equatorial Pacific and cooling on both sides of the equator, suggesting a more confined warming in the future scenario than over the historical period (Fig. 12b). The CT La Niña changes exhibit cooling in the west and warming in the east equatorial Pacific (Fig. 12c). The WP La Niña pattern suggests strengthening of the cold events in a warmer scenario (Fig. 12d). However, these future changes in the amplitude of ENSO events are overall small and not consistent across the models. Analysis of the spatial metrics shown in Fig. 3 reveals no clear change in the multimodel mean magnitude or location of maximum SST anomaly. The westward extent of

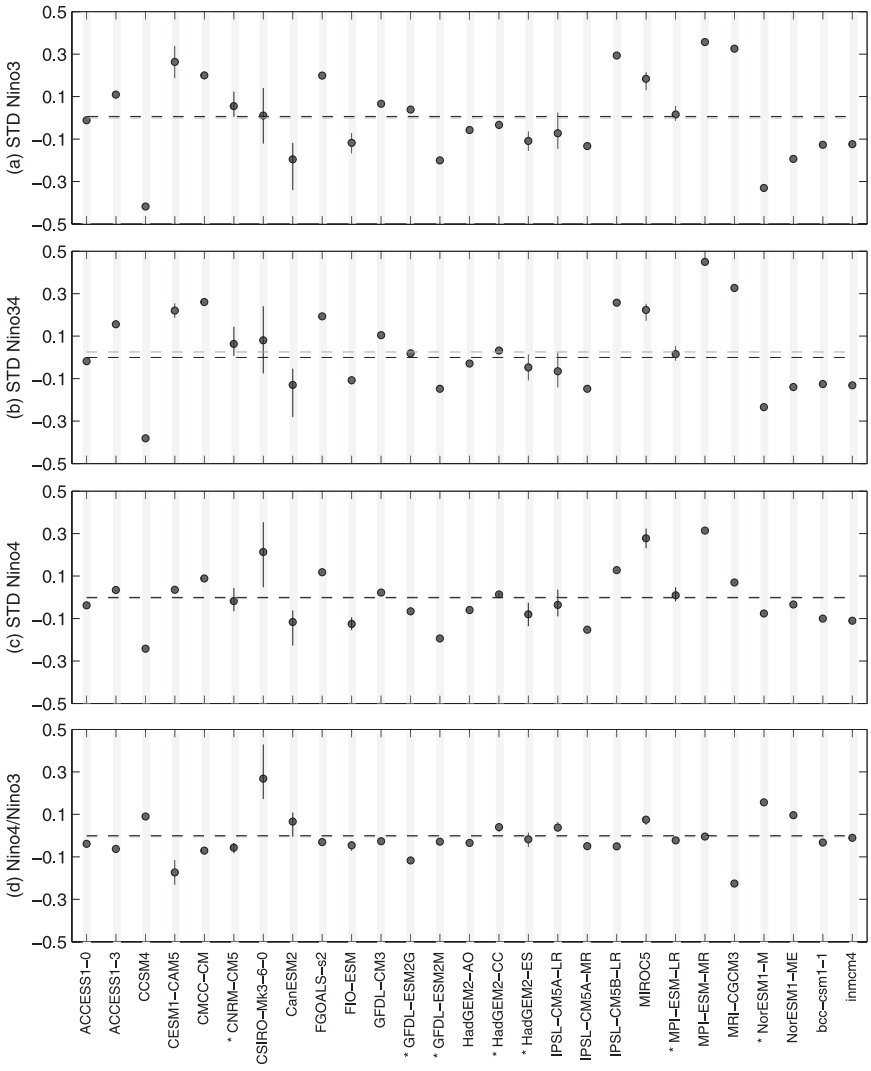

FIG. 13. Difference in the standard deviation of (a) Niño-3, (b) Niño-3.4, and (c) Niño-4 indices between RCP8.5 and historical simulations for 27 CMIP5 models. (d) Difference in the ratio of the standard deviation between Niño-4 and Niño-3. The gray dashed line represents the difference in the multimodel mean; zero appears as the black dashed line. Vertical bars represent the range of ensemble members when available and circles the respective ensemble mean.

ENSO also does not show significant changes in the future projections, except for CT La Niña events that extend 15° westward on average, which is consistent with the cooling around the date line shown in Fig. 12c.

The change in the amplitude of SST anomalies is also quantified in Fig. 13 via the difference between the standard deviation of Niño indices from the historical period to the RCP8.5 scenario. There is little agreement in the projections of Niño indices across the models, indicating that the changes derived for the multimodel mean (Fig. 12) are not statistically significant. Our analysis based on 27 CMIP5 models does not reveal any enhancement of WP to CT ENSO intensity from historical to RCP8.5 scenario (Fig. 13d). This contradicts the findings of Kim and Yu (2012), who reported increased WP to CT intensity ratio from historical to RCP4.5 scenario using a smaller set of CMIP5 models. In particular, the Niño-4 to Niño-3 ratio averaged for 16 out of 20 models in common with Kim and Yu (2012) exhibits an 1.3% increase from the historical period to the RCP8.5 simulation; while the ratio averaged for their "7 models that best represent CT and WP ENSO" (see asterisks in Fig. 13) reveals a decrease of 0.9%; however, both numbers are nonsignificant. It is also important to note that Kim and Yu (2012) analyze RCP4.5 simulations while we have assessed the RCP8.5 scenario.

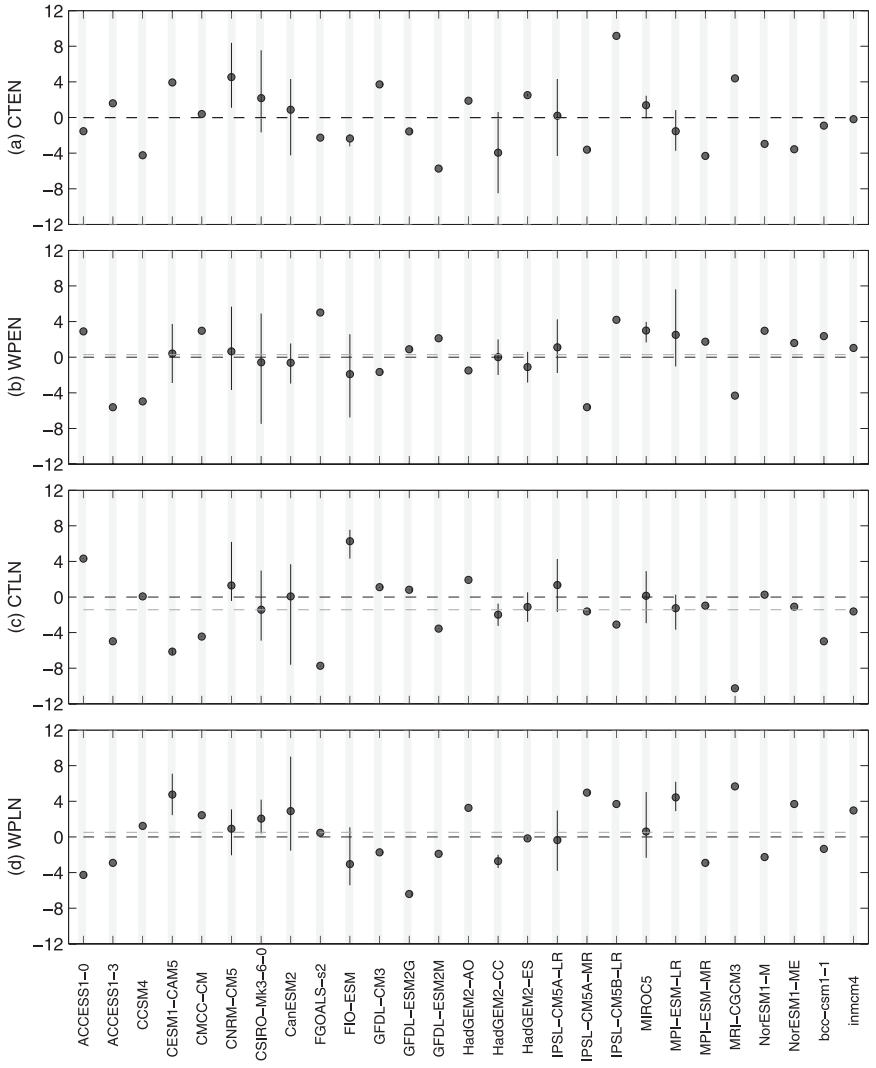

FIG. 14. Difference in the number of events $(100\,\mathrm{yr})^{-1}$ between RCP8.5 and historical simulations for 27 CMIP5 models: (a) CT El Niño, (b) WP El Niño, (c) CT La Niña, and (d) WP La Niña. The gray dashed line represents the difference in the multimodel mean; zero appears as the black dashed line. Vertical bars represent the range of ensemble members when available and circles the respective ensemble mean.

When individual models are considered, the WP to CT ENSO asymmetry in regard to intensity can show significant changes: for instance, there is a robust increase in the Niño-4/Niño-3 ratio for all 10 members of the CSIRO Mk3.6.0 model, 5 members of the CanESM2 model, and 3 members of the MIROC5 model. Our results support the findings of Stevenson (2012), who found no robust change in the multimodel mean SST difference between the Niño-4 and Niño-3.4 regions from twentieth century to RCP4.5, except when individual models are examined: that is, 4 of the 11 CMIP5 models containing more than three members reveal statistically significant changes. This shows the importance of considering large ensembles when examining the robustness of ENSO projections.

An evaluation of the frequency of ENSO events from historical to RCP8.5 scenarios shows no significant result (Fig. 14). The evolution of ENSO events also exhibits little change in the future. On average, the timing of the initiation, peak, and termination of the Pacific events show similar behavior in the RCP8.5 scenario compared to the historical period (Fig. 9b, red and blue curves).

5. Discussion and conclusions

Now as in the past there remain substantial problems in the realistic simulation of ENSO in climate models, despite good progress over the past decade. Of particular importance for ENSO teleconnections is the correct

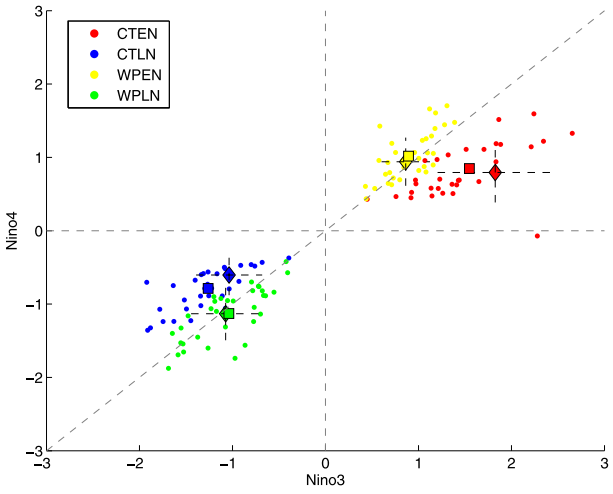

FIG. 15. Scatterplot of averaged DJF Niño-4 × Niño-3 indices for each model and each ENSO category: CT El Niños (red dots), WP El Niños (yellow dots), CT La Niñas (blue dots), and WP La Niñas (green dots); squares represent HadISST data and diamonds are the multimodel mean. Dashed lines represent the spread across CMIP5 models and observed events.

simulation of the characteristics of different ENSO flavors, classified here into cold tongue and warm pool El Niños and La Niñas. This study assesses ENSO in 34 CMIP5 models and finds that, while most models do simulate events that can be classed as either CT or WP, there is varying fidelity across the models.

Similar to observations, the CT and WP El Niños are easily distinguishable in most CMIP5 models; however, the two types of La Niña are much less so. The scatter diagram of Niño indices in Fig. 15 illustrates this relationship in the CMIP5 models: the larger the linearity between Niño-3 and Niño-4 indices, the less independent the events. This result corroborates the findings of Kug and Ham (2011), who reported that CMIP3 models simulate more distinct types of El Niño than La Niña. However, when looking at individual models, over one-third of CMIP5 models represent the two types of La Niña events (see models with similar numbers of CT and WP La Niñas in Fig. 1); for this reason we have assessed La Niñas separately in this study.

The CMIP5 models can simulate the intensity and location of maximum SST anomalies during ENSO events within the observational bounds. This result is consistent with the findings by Kim and Yu (2012), who reported a good representation of WP ENSO intensity, with relatively more biases for CT ENSOs. Our assessment of 34 CMIP5 models indicates that, while the intensity of the four ENSO types is in general realistically represented, the spatial pattern of warm and cold events (particularly WP events) extend farther west in the simulations compared to observations (Table 3).

The observed asymmetries in the intensity between warm and cold events (i.e., El Niños stronger than La Niñas) and between warm events (i.e., CT stronger than WP El Niños) are captured in most of the CMIP5 models analyzed here. However, most of the models fail to reproduce the observed asymmetry between the cold events: that is, simulated CT La Niñas are stronger than WP La Niñas (note the limitation due to the small observed number of CT La Niñas).

Most CMIP5 models can simulate an evolution of CT El Niño events that is similar to that observed, with correct time of initiation, duration, and peak in December. The simulated CT El Niños are often followed by cold events one year after the peak of the warm event in most of the models, while cold events more commonly occur two years after in observations. The duration of WP El Niños is overestimated for most of the models, a bias related to the simulated wind stress anomalies in the central to western equatorial Pacific being too strong and persistent. In general, the evolution of cold events also exhibits biases, with the simulated CT La Niñas starting about two seasons later than observed and WP La Niñas ending approximately six months earlier than observed. It is important to note, however, that a fair amount of variability exists in the life cycle of individual events: that is, not all El Niños and La Niñas exhibit equal duration. Thus, one should be cautious given the small sample size of observed events (especially for CT La Niñas) and the different duration of individual events.

The seasonality of ENSO shows varying degrees of fidelity depending on the Niño region. Better agreement in the timing of ENSO peak among CMIP5 models is seen in the Niño-3.4 region (27 of 34 models peak in the correct season) while a large spread occurs in the Niño-3 region (only $\sim 1/3$ of the models peak in the correct season). Even in models where the peak of the Pacific SST variability is simulated in December, good skill in simulating other aspects of ENSO seasonality is not guaranteed. Several models show an overly weak seasonality, suggesting that many ENSO events are also occurring at the wrong time of year. Particularly in the Niño-3 and Niño-4 regions, ENSO events in many CMIP5 models peak in the wrong seasons.

The seasonality of ENSO is an important feature that determines the timing of the evolution of warm and cold events. Lengaine and Vecchi (2010) showed that the seasonality has been linked to the termination of strong El Niño events in CMIP3 models. This also seems to be the case for CMIP5 models; that is, the larger the ENSO seasonality, the better the timing of the termination, particularly for CT and WP warm events (not shown). The substantial spread in the seasonal peak and termination timing of ENSO events in CMIP5 models compared to

observations suggests that ENSO seasonality is still an aspect that needs to be improved in models.

Most of the biases in the ENSO SST anomalies can be linked to biases in the wind stress anomalies, which are likely in turn related to mean state biases in the SST. For all ENSO flavors the wind stress extends too far westward, particularly during WP events. These biases in the wind stress anomalies generate spurious thermocline anomalies that propagate eastward as upwelling and downwelling Kelvin waves, which can in turn influence the evolution of ENSO events. It is noted here that spurious thermocline anomalies over the central Pacific may influence the evolution of warm pool events in the models. Furthermore, the narrower meridional extent of the CT ENSO wind stress anomalies seen in the multimodel mean likely contributes to the more rapid and somewhat more regular ENSO phase transition. This systematic bias was also seen in CMIP3 models (Capotondi et al. 2006), which is likely to be associated with the classical cold tongue problem, requiring improvements in the representation of the physics of the coupled climate system (e.g., Guilyardi et al. 2009a). Lengaigne and Vecchi (2010) found that only four CMIP3 models are able to represent the observed termination of moderate and extreme El Niño events, with the westward and eastward propagation of the SST anomalies, respectively. In this study, all of the analyzed CMIP5 models exhibit an eastward propagation of SST anomalies in the termination phase of WP El Niños (not shown). Although we have not explicitly separated each type of event into strong or weak, our ENSO classification into WP and CT El Niños also acts to differentiate events by strength in the observations. In the CMIP5 models, however, the WP El Niños are generally stronger than observed, and the dissipation of the anomalies occurs through similar processes in both events.

Ham and Kug (2012) and Kug et al. (2012) showed that the representation of ENSO into CT and WP events in climate models is sensitive to the atmospheric response, in particular to the location of convection, to the underlying SST anomaly patterns. Bellenger et al. (2013) also demonstrated that convection parameterization in climate models can strongly affect the seasonal phase locking of ENSO. Watanabe et al. (2012) reported that a wetter mean state with higher precipitation in the eastern Pacific leads to a larger ENSO amplitude as a result of a stronger positive coupled feedback. In our analysis, the biases in wind stress anomalies (also related to precipitation) may act to enhance the coupling between the atmosphere and the SST in the CMIP5 models, resulting in a larger than observed WP El Niño amplitude in western Pacific. As a consequence, the dissipation of the WP events seems to occur via ocean heat discharge, in a similar way to CT events, rather than via advection of mean SST gradients by anomalous zonal currents as seen in observations.

Recent studies have also attributed biases in ENSO simulations to remote influences, particularly climate over the Indian Ocean basin (Du et al. 2013; Santoso et al. 2012, and references therein). Okumura and Deser (2010) suggest that remote forcing from the Indian Ocean can influence the asymmetry in the duration of El Niño and La Niña. Thus, some of the modeled ENSO biases reported here could relate to how CMIP5 models simulate Indian Ocean climate and its variability.

The different types of ENSO do not show robust changes in the spatial pattern, even when subject to large changes in radiative forcing. In addition, no consistent changes are seen in the WP–CT ratio or in the frequency of ENSO events. This result is consistent with previous studies based on CMIP3 that concluded there is little agreement among the models for projected ENSO changes (e.g., van Oldenborgh et al. 2005; Guilyardi 2006; Collins et al. 2010; Stevenson 2012) and is also consistent with the idea that changes in ENSO amplitude and frequency can be hard to detect given the level of natural variability present in the climate system (e.g., Wittenberg 2009; Aiken et al. 2013).

In summary, our study suggests that CMIP5 models can simulate the two types of ENSO with varying degrees of fidelity. The features that models represent well include (i) stronger El Niños than La Niñas; (ii) stronger CT El Niños than WP El Niños; (iii) the location of maximum SST anomaly for all events; (iv) the magnitude of CT and WP events; (v) the ENSO peak around December; and (vi) the time evolution of CT El Niño events. On the other hand, the majority of models (i) cannot simulate the asymmetry between cold events (stronger CT than WP La Niñas); (ii) overestimate wind stress in the western Pacific; (iii) simulate SST anomalies extending too far west in the equatorial Pacific; (iv) agree poorly on the ENSO seasonal evolution; and (v) overestimate the termination duration of WP El Niño and underestimate for WP La Niña. Finally, there are no robust changes in the future projections of the magnitude or location of maximum SST anomalies, nor the frequency of ENSO events. This study motivates further analyses to understand the disagreement among models and projections, via assessments of climate simulations remote from the tropical Pacific, as well as understanding the feedback mechanisms operating in the Pacific region in CMIP5 models.

Acknowledgments. We acknowledge the WCRP's Working Group on Coupled Modelling, which is responsible for CMIP, and we thank the climate modeling

groups for producing and making available their model output. The U.S. DOE's PCMDI provided coordinating support and led development of software infrastructure in partnership with the Global Organization for Earth System Science Portals. This work was also supported by the NCI National Facility at the ANU via the provision of computing resources to the ARC Centre of Excellence for Climate System Science. We acknowledge all the Institutions responsible for the observations and reanalysis products for having made their data available. This project was supported by the Australian Research Council.

REFERENCES

Aiken, C. M., A. Santoso, S. McGregor, and M. H. England, 2013: The 1970's shift in ENSO dynamics: A linear inverse model perspective. *Geophys. Res. Lett.,* **40,** 1612–1617, doi:10.1002/grl.50264.

An, S.-I., and F.-F. Jin, 2004: Nonlinearity and asymmetry of ENSO. *J. Climate,* **17,** 2399–2412, doi:10.1175/1520-0442(2004)017<2399:NAAOE>2.0.CO;2.

Ashok, K., S. K. Behera, S. A. Rao, H. Weng, and T. Yamagata, 2007: El Niño Modoki and its possible teleconnection. *J. Geophys. Res.,* **112,** C11007, doi:10.1029/2006JC003798.

Battisti, D. S., and A. C. Hirst, 1989: Interannual variability in the tropical atmosphere–ocean model: Influence of the basic state, ocean geometry, and nonlinearity. *J. Atmos. Sci.,* **46,** 1687–1712, doi:10.1175/1520-0469(1989)046<1687:IVIATA>2.0.CO;2.

Bellenger, H., E. Guilyardi, J. Leloup, M. Lengaigne, and J. Vialard, 2013: ENSO representation in climate models: From CMIP3 to CMIP5. *Climate Dyn.,* doi:10.1007/s00382-013-1783-z.

Burgers, G., and D. B. Stephenson, 1999: The "normality" of El Niño. *Geophys. Res. Lett.,* **26,** 1027–1030, doi:10.1029/1999GL900161.

Capotondi, A., A. Wittenberg, and S. Masina, 2006: Spatial and temporal structure of tropical Pacific interannual variability in 20th century coupled simulations. *Ocean Modell.,* **15,** 274–298, doi:10.1016/j.ocemod.2006.02.004.

Carton, J. A., and B. S. Giese, 2008: A reanalysis of ocean climate using Simple Ocean Data Assimilation (SODA). *Mon. Wea. Rev.,* **136,** 2999–3017, doi:10.1175/2007MWR1978.1.

Choi, J., S.-I. An, J.-S. Kug, and S.-W. Yeh, 2011: The role of mean state on changes in El Niño's flavor. *Climate Dyn.,* **37,** 1205–1215, doi:10.1007/s00382-010-0912-1.

——, ——, and S.-W. Yeh, 2012: Decadal amplitude modulation of two types of ENSO and its relationship with the mean state. *Climate Dyn.,* **38,** 2631–2644, doi:10.1007/s00382-011-1186-y.

Collins, M., and Coauthors, 2010: The impact of global warming on the tropical Pacific Ocean and El Niño. *Nat. Geosci.,* **3,** 391–397, doi:10.1038/ngeo868.

Dewitte, B., J. Choi, S.-I. An, and S. Thual, 2012: Vertical structure variability and equatorial waves during central Pacific and eastern Pacific El Niños in a coupled general circulation model. *Climate Dyn.,* **38,** 2275–2289.

Dommenget, D., T. Bayr, and C. Frauen, 2013: Analysis of the non-linearity in the pattern and time evolution of El Niño Southern Oscillation. *Climate Dyn.,* **40,** 2825–2847, doi:10.1007/s00382-012-1475-0.

Du, Y., S.-P. Xie, Y.-L. Yang, X.-T. Zheng, L. Liu, and G. Huang, 2013: Indian Ocean variability in the CMIP5 multimodel ensemble: The basin mode. *J. Climate,* **26,** 7240–7266, doi:10.1175/JCLI-D-12-00678.1.

Frauen, C., and D. Dommenget, 2010: El Niño and La Niña amplitude asymmetry caused by atmospheric feedbacks. *Geophys. Res. Lett.,* **37,** L18801, doi:10.1029/2010GL044444.

Guilyardi, E., 2006: El Niño–mean state–seasonal cycle interactions in a multi-model ensemble. *Climate Dyn.,* **26,** 329–348, doi:10.1007/s00382-005-0084-6.

——, P. Braconnot, F.-F. Jin, S. T. Kim, M. Kolasinski, T. Li, and I. Musat, 2009a: Atmosphere feedbacks during ENSO in a coupled GCM with a modified atmospheric convection scheme. *J. Climate,* **22,** 5698–5718, doi:10.1175/2009JCLI2815.1.

——, A. Wittenberg, A. Fedorov, M. Collins, C. Wang, A. Capotondi, G. J. van Oldenborgh, and T. Stockdale, 2009b: Understanding El Niño in ocean–atmosphere general circulation models. *Bull. Amer. Meteor. Soc.,* **90,** 325–340, doi:10.1175/2008BAMS2387.1.

——, W. Cai, M. Collins, A. Fedorov, F.-F. Jin, A. Kumar, D.-Z. Sun, and A. Wittenberg, 2012: New strategies for evaluating ENSO processes in climate models. *Bull. Amer. Meteor. Soc.,* **93,** 235–238, doi:10.1175/BAMS-D-11-00106.1.

Ham, Y.-G., and J.-S. Kug, 2012: How well do current climate models simulate two types of El Niño? *Climate Dyn.,* **39,** 383–398, doi:10.1007/s00382-011-1157-3.

Hoerling, M. P., A. Kumar, and M. Zhong, 1997: El Niño, La Niña, and the nonlinearity of their teleconnections. *J. Climate,* **10,** 1769–1786, doi:10.1175/1520-0442(1997)010<1769:ENOLNA>2.0.CO;2.

Hu, Z.-Z., A. Kumar, B. Jha, W. Wang, B. Huang, and B. Huang, 2012: An analysis of warm pool and cold tongue El Niños: Air–sea coupling processes, global influences, and recent trends. *Climate Dyn.,* **38,** 2017–2035, doi:10.1007/s00382-011-1224-9.

Jin, F.-F., 1997: An equatorial ocean recharge paradigm for ENSO. Part I: Conceptual model. *J. Atmos. Sci.,* **54,** 811–829, doi:10.1175/1520-0469(1997)054<0811:AEORPF>2.0.CO;2.

Johnson, N. C., 2013: How many ENSO flavors can we distinguish? *J. Climate,* **26,** 4816–4827, doi:10.1175/JCLI-D-12-00649.1.

Jourdain, N. C., A. Sen Gupta, A. S. Taschetto, C. C. Ummenhofer, A. F. Moise, and K. Ashok, 2013: The Indo-Australian monsoon and its relationship to ENSO and IOD in reanalysis data and the CMIP3/CMIP5 simulations. *Climate Dyn.,* **41,** 3073–3102.

Kalnay, E., and Coauthors, 1996: The NCEP/NCAR 40-Year Reanalysis Project. *Bull. Amer. Meteor. Soc.,* **77,** 437–472, doi:10.1175/1520-0477(1996)077<0437:TNYRP>2.0.CO;2.

Kang, I.-S., and J.-S. Kug, 2002: El Niño and La Niña sea surface temperature anomalies: Asymmetry characteristics associated with their wind stress anomalies. *J. Geophys. Res.,* **107,** 4372, doi:10.1029/2001JD000393.

Kim, J., K. Kim, and S. Yeh, 2012: Statistical evidence for the natural variation of the central Pacific El Niño. *J. Geophys. Res.,* **117,** C06014, doi:10.1029/2012JC008003.

Kim, S. T., and F. Jin, 2011: An ENSO stability analysis. Part II: Results from the twentieth and twenty-first century simulations of the CMIP3 models. *Climate Dyn.,* **36,** 1609–1627, doi:10.1007/s00382-010-0872-5.

——, and J.-Y. Yu, 2012: The two types of ENSO in CMIP5 models. *Geophys. Res. Lett.,* **39,** L11704, doi:10.1029/2012GL052006.

Kirtman, B. P., 1997: Oceanic Rossby wave dynamics and the ENSO period in a coupled model. *J. Climate,* **10,** 1690–1704, doi:10.1175/1520-0442(1997)010<1690:ORWDAT>2.0.CO;2.

Kug, J.-S., and Y.-G. Ham, 2011: Are there two types of La Niña? *Geophys. Res. Lett.,* **38,** L16704, doi:10.1029/2011GL048237.

——, F.-F. Jin, and S.-I. An, 2009: Two types of El Niño events: Cold tongue El Niño and warm pool El Niño. *J. Climate,* **22,** 1499–1515, doi:10.1175/2008JCLI2624.1.

——, Y.-G. Ham, J.-Y. Lee, and F.-F. Jin, 2012: Improved simulation of two types of El Niño in CMIP5 models. *Environ. Res. Lett.,* **7,** 034002, doi:10.1088/1748-9326/7/3/034002.

Larkin, N. K., and D. E. Harrison, 2002: ENSO warm (El Niño) and cold (La Niña) event life cycles: Ocean surface anomaly patterns, their symmetries, asymmetries, and implications. *J. Climate,* **15,** 1118–1140, doi:10.1175/1520-0442(2002)015<1118:EWENOA>2.0.CO;2.

Lee, T., and M. J. McPhaden, 2010: Increasing intensity of El Niño in the central-equatorial Pacific. *Geophys. Res. Lett.,* **37,** L14603, doi:10.1029/2010GL044007.

Leloup, J., M. Lengaigne, and J.-P. Boulanger, 2008: Twentieth century ENSO characteristics in the IPCC database. *Climate Dyn.,* **30,** 277–291, doi:10.1007/s00382-007-0284-3.

Lengaigne, M., and G. Vecchi, 2010: Contrasting the termination of moderate and extreme El Niño events in coupled general circulation models. *Climate Dyn.,* **35,** 299–313, doi:10.1007/s00382-009-0562-3.

Lian, T., and D. Chen, 2012: An evaluation of rotated EOF analysis and its application to tropical Pacific SST variability. *J. Climate,* **25,** 5361–5373, doi:10.1175/JCLI-D-11-00663.1.

McGregor, S., A. Timmermann, S. Schneider, M. F. Stuecker, and M. H. England, 2012: The effect of the South Pacific convergence zone on the termination of El Niño events and the meridional asymmetry of ENSO. *J. Climate,* **25,** 5566–5586, doi:10.1175/JCLI-D-11-00332.1.

——, N. Ramesh, P. Spence, M. H. England, M. J. McPhaden, and A. Santoso, 2013: Meridional movement of wind anomalies during ENSO events and their role in event termination. *Geophys. Res. Lett.,* **40,** 749–754, doi:10.1002/grl.50136.

McPhaden, M. J., and X. Zhang, 2009: Asymmetry in zonal phase propagation of ENSO sea surface temperature anomalies. *Geophys. Res. Lett.,* **36,** L13703, doi:10.1029/2009GL038774.

——, and Coauthors, 1998: The Tropical Ocean-Global Atmosphere observing system: A decade of progress. *J. Geophys. Res.,* **103** (C7), 14 169–14 240, doi:10.1029/97JC02906.

——, T. Lee, and D. McClurg, 2011: El Niño and its relationship to changing background conditions in the tropical Pacific Ocean. *Geophys. Res. Lett.,* **38,** L15709, doi:10.1029/2011GL048275.

Meinen, C. S., and M. J. McPhaden, 2000: Observations of warm water volume changes in the equatorial Pacific and their relationship to El Niño and La Niña. *J. Climate,* **13,** 3551–3559, doi:10.1175/1520-0442(2000)013<3551:OOWWVC>2.0.CO;2.

Na, H., B.-G. Jang, W.-M. Choi, and K.-Y. Kim, 2011: Statistical simulations of the future 50-year statistics of cold-tongue El Niño and warm-pool El Niño. *Asia-Pac. J. Atmos. Sci.,* **47,** 223–233, doi:10.1007/s13143-011-0011-1.

Newman, M., S.-I. Shin, and M. A. Alexander, 2011: Natural variation in ENSO flavors. *Geophys. Res. Lett.,* **38,** L14705, doi:10.1029/2011GL047658.

Ohba, M., and H. Ueda, 2009: Role of nonlinear atmospheric response to SST on the asymmetric transition process of ENSO. *J. Climate,* **22,** 177–192, doi:10.1175/2008JCLI2334.1.

——, D. Nohara, and H. Ueda, 2010: Simulation of asymmetric ENSO transition in WCRP CMIP3 multimodel experiments. *J. Climate,* **23,** 6051–6067, doi:10.1175/2010JCLI3608.1.

Okumura, Y. M., and C. Deser, 2010: Asymmetry in the duration of El Niño and La Niña. *J. Climate,* **23,** 5826–5843, doi:10.1175/2010JCLI3592.1.

——, M. Ohba, C. Deser, and H. Ueda, 2011: A proposed mechanism for the asymmetric duration of El Niño and La Niña. *J. Climate,* **24,** 3822–3829, doi:10.1175/2011JCLI3999.1.

Rayner, N. A., D. E. Parker, E. B. Horton, C. K. Folland, L. V. Alexander, D. P. Rowell, E. C. Kent, and A. Kaplan, 2003: Global analyses of sea surface temperature, sea ice, and night marine air temperature since the late nineteenth century. *J. Geophys. Res.,* **108,** 4407, doi:10.1029/2002JD002670.

Rodgers, K. B., P. Friederichs, and M. Latif, 2004: Tropical Pacific decadal variability and its relation to decadal modulations of ENSO. *J. Climate,* **17,** 3761–3774, doi:10.1175/1520-0442(2004)017<3761:TPDVAI>2.0.CO;2.

Santoso, A., M. H. England, and W. Cai, 2012: Impact of Indo-Pacific feedback interactions on ENSO dynamics diagnosed using ensemble climate simulations. *J. Climate,* **25,** 7743–7763.

Schopf, P. S., and R. J. Burgman, 2006: A simple mechanism for ENSO residuals and asymmetry. *J. Climate,* **19,** 3167–3179, doi:10.1175/JCLI3765.1.

Stevenson, S. L., 2012: Significant changes to ENSO strength and impacts in the twenty-first century: Results from CMIP5. *Geophys. Res. Lett.,* **39,** L17703, doi:10.1029/2012GL052759.

Su, J., R. Zhang, T. Li, X. Rong, J.-S. Kug, and C.-C. Hong, 2010: Causes of the El Niño and La Niña amplitude asymmetry in the equatorial eastern Pacific. *J. Climate,* **23,** 605–617, doi:10.1175/2009JCLI2894.1.

Suarez, M. J., and P. S. Schopf, 1988: A delayed action oscillator for ENSO. *J. Atmos. Sci.,* **45,** 3283–3287, doi:10.1175/1520-0469(1988)045<3283:ADAOFE>2.0.CO;2.

Sun, F., and J.-Y. Yu, 2009: A 10–15-Yr modulation cycle of ENSO intensity. *J. Climate,* **22,** 1718–1735, doi:10.1175/2008JCLI2285.1.

Takahashi, K., A. Montecinos, K. Goubanova, and B. Dewitte, 2011: ENSO regimes: Reinterpreting the canonical and Modoki El Niño. *Geophys. Res. Lett.,* **38,** L10704, doi:10.1029/2011GL047364.

Taschetto, A. S., and M. H. England, 2009: El Niño Modoki impacts on Australian rainfall. *J. Climate,* **22,** 3167–3174, doi:10.1175/2008JCLI2589.1.

——, C. C. Ummenhofer, A. Sen Gupta, and M. H. England, 2009: Effect of anomalous warming in the central Pacific on the Australian monsoon. *Geophys. Res. Lett.,* **36,** L12704, doi:10.1029/2009GL038416.

——, R. J. Haarsma, A. Sen Gupta, C. C. Ummenhofer, K. J. Hill, and M. H. England, 2010: Australian monsoon variability driven by a Gill–Matsuno-type response to central west Pacific warming. *J. Climate,* **23,** 4717–4736, doi:10.1175/2010JCLI3474.1.

Taylor, K. E., R. J. Stouffer, and G. A. Meehl, 2012: An Overview of CMIP5 and the experiment design. *Bull. Amer. Meteor. Soc.,* **93,** 485–498, doi:10.1175/BAMS-D-11-00094.1.

Trenberth, K. E., and L. Smith, 2009: Variations in the three-dimensional structure of the atmospheric circulation with different flavors of El Niño. *J. Climate,* **22,** 2978–2991, doi:10.1175/2008JCLI2691.1.

van Oldenborgh, G. J., S. Y. Philip, and M. Collins, 2005: El Niño in a changing climate: A multi-model study. *Ocean Sci.,* **1,** 81–95, doi:10.5194/os-1-81-2005.

Watanabe, M., J.-S. Kug, F.-F. Jin, M. Collins, M. Ohba, and A. T. Wittenberg, 2012: Uncertainty in the ENSO amplitude change from the past to the future. *Geophys. Res. Lett.,* **39,** L20703, doi:10.1029/2012GL053305.

Weng, H., K. Ashok, S. K. Behera, S. A. Rao, and T. Yamagata, 2007: Impacts of recent El Niño Modoki on dry/wet conditions in the Pacific Rim during boreal summer. *Climate Dyn.,* **29,** 113–129, doi:10.1007/s00382-007-0234-0.

Wittenberg, A. T., 2009: Are historical records sufficient to constrain ENSO simulations? *Geophys. Res. Lett.,* **36,** L12702, doi:10.1029/2009GL038710.

Yeh, S.-W., and B. P. Kirtman, 2004: Tropical Pacific decadal variability and ENSO amplitude modulation in a CGCM. *J. Geophys. Res.,* **109,** C11009, doi:10.1029/2004JC002442.

——, J.-S. Kug, B. Dewitte, M. H. Kwon, and B. P. Kirtman, 2009: El Niño in a changing climate. *Nature,* **461,** 511–514, doi:10.1038/nature08316.

——, B. P. Kirtman, J.-S. Kug, W. Park, and M. Latif, 2011: Natural variability of the central Pacific El Niño event on multi-centennial timescales. *Geophys. Res. Lett.,* **38,** L02704, doi:10.1029/2010GL045886.

——, Y.-G. Ham, and J.-Y. Lee, 2012: Changes in the tropical Pacific SST trend from CMIP3 to CMIP5 and its implication of ENSO. *J. Climate,* **25,** 7764–7771, doi:10.1175/JCLI-D-12-00304.1.

Yu, J.-Y., and S. T. Kim, 2010: Identification of central-Pacific and eastern-Pacific types of ENSO in CMIP3 models. *Geophys. Res. Lett.,* **37,** L15705, doi:10.1029/2010GL044082.

——, and ——, 2011: Reversed spatial asymmetries between El Niño and La Niña and their linkage to decadal ENSO modulation in CMIP3 models. *J. Climate,* **24,** 5423–5434, doi:10.1175/JCLI-D-11-00024.1.

Zebiak, S. E., 1989: Oceanic heat content variability and El Niño cycles. *J. Phys. Oceanogr.,* **19,** 475–486, doi:10.1175/1520-0485(1989)019<0475:OHCVAE>2.0.CO;2.